Predicting the Starquakes in PSR J0537−6910
August 15, 2011 at 1291 minutes VERSION

J. Middleditch[1], F. E. Marshall[2], Q. D. Wang[3], E. V. Gotthelf[4], and W. Zhang[2]

jon@lanl.gov

ABSTRACT

We report the results of 12.5 years of monitoring of PSR J0537−6910, the 16 ms pulsar in the Large Magellanic Cloud, using data acquired with the Rossi X-ray Timing Explorer. During this campaign the pulsar experienced 41 sudden increases in frequency ("glitches" – 38 with increases of at least five μHz) amounting to a total gain of ten parts per million of rotation frequency superposed on its gradual spindown of $\dot{\nu} = -2 \times 10^{-10}$ Hz s^{-1}. The time interval from one glitch to the next obeys a strong linear correlation to the amplitude of the first glitch, with a mean slope of about 400 days per part per million (6.5 days per μHz), such that these intervals can be predicted to within a few days, an accuracy which has never before been seen in any other pulsar. There appears to be an upper limit of $\sim$40 μHz for the size of glitches in *all* pulsars, with the 1999 April glitch of PSR J0537−6910 as the largest so far. The change of its spindown across the glitches, $\Delta\dot{\nu}$, appears to have the same hard lower limit of -1.5 $\times 10^{-13}$ Hz s^{-1}, as, again, that observed in all other pulsars. The spindown continues to increase in the long term, $\ddot{\nu}$ = -10^{-21} Hz s^{-2}, and thus the timing age of PSR J0537−6910 ($-0.5\nu\dot{\nu}^{-1}$) continues to decrease at a rate of nearly one year every year, consistent with movement of its magnetic moment away from its rotational axis by one radian every 10,000 years, or about one meter per year. PSR J0537−6910 was likely to have been born as a nearly-aligned rotator

[1]Modeling, Algorithms, & Informatics, CCS-3, MS B265, Computer, Computational, & Statistical Sciences Division, Los Alamos National Laboratory, Los Alamos, NM 87545; jon@lanl.gov

[2]Laboratory for High Energy Astrophysics, Goddard Space Flight Center, Greenbelt, MD 20771; frank.marshall@gsfc.nasa.gov, William.W.Zhang@nasa.gov

[3]Department of Astronomy, University of Massachusetts, B-524, LGRT, Amherst, MA 01003; wqd@astro.umass.edu

[4]Columbia Astrophysical Laboratory, Columbia University, 550 West 120th Street, New York, NY 10027; eric@astro.columbia.edu

spinning at 75–80 Hz, with a $|\dot{\nu}|$ considerably smaller than its current value of 2×10^{-10} Hz s^{-1}. Its pulse profile consists of a single pulse which is found to be flat at its peak for at least 0.02 cycles. Glitch activity may grow exponentially with a timescale of 170 years $\nu\dot{\nu}$ $((\nu\dot{\nu})_{Crab})^{-1}$ in all young pulsars.

Subject headings: pulsars:neutron—stars:individual (PSR J0537−6910)—X-rays:stars

1. Introduction

The X-ray pulsar, PSR J0537−6910 (hereafter J0537), in the 30 Doradus star formation region of the Large Magellanic Cloud (LMC), was discovered serendipitously in an observation of Supernova 1987A with the Rossi X-Ray Timing Explorer (RXTE) in a search for its pulsar remnant (Marshall et al. 1998; Middleditch et al. 2000). Associated with the 4,000-year old LMC supernova remnant, N157B (Wang & Gotthelf 1998), with a rotation period of only 16.1 ms (62 Hz), it is the fastest rotating young pulsar known, the next fastest two young pulsars being the Crab pulsar, with a period of 33 ms (30 Hz), and PSR B0540-69, with a period of 50 ms (20 Hz). With a spindown rate near -2×10^{-10} Hz s^{-1}, J0537 has one of the highest energy loss rates known, of $\sim 5\times10^{38} I_{45}$ ergs s^{-1}, where I_{45} is the moment of inertia of the neutron star (NS) in units of 10^{45} g cm^2, but it has so far only been detected in the X-ray band despite several radio and optical searches (Crawford et al. 1998; Mignani et al. 2000).

Pulsars are known for their very stable rotation and small spindown rates, and their spindown histories can be used to constrain models of their emission mechanisms. Characteristic pulsar ages, τ_c, may be estimated, assuming that their spindowns are dominated by magnetic dipole radiation, $\dot{\nu} \propto \nu^3$, as $\tau_c \equiv -0.5\nu\dot{\nu}^{-1}$, where ν is the rotation rate in cycles s^{-1} (Hz), and $\dot{\nu}$ is its (almost always negative) time derivative, or spindown, in Hz s^{-1}. J0537 has a young characteristic timing age of 5×10^3 years, consistent with the 4,000-yr estimated age of N157B, though we have showed this quantity to be actually decreasing with time (Marshall et al. 2004, hereafter M04).

Many pulsars have also been shown to undergo sudden discontinuities (usually increases) in their rotation rates known as "glitches," (see, e.g., Alpar et al. 1993,1996; Hobbs et al. 2002; Johnston et al. 1995; Jones 2002; Lyne, Pritchard, & Smith 1993; Lyne et al. 2000; Pines & Alpar 1985; Ruderman, Zhu, & Chen 1998; Shemar & Lyne 1996; Wang et al. 2000; Wang et al. 2001a; and Wong, Backer, & Lyne 2001). Although glitches have been detected in both young and old pulsars, they are predominately found in the younger ones ($\tau_c < 10^5$ yr, Urama and Okeke 1999, Lyne, Shemar, & Smith 2000). Glitches are thought to occur

when angular momentum is transferred from a more rapidly rotating component of the NS to the outer crust (see also Anderson & Itoh 1975; Franco, Link, & Epstein 2000; and §5.1 for alternative models).

The increase in rotation rate shows up within a few minutes because the NS star magnetic field is thought to be fixed in the crust. Thus, in addition to the continuous spindown of a pulsar, glitches can be used to reveal details about the NS equation of state and internal structure, which would otherwise remain hidden (see, e.g., Datta & Alpar 1993; Link, Epstein, & Lattimer 1999). If, for example, erratic timing activity was found to always precede the large glitches, as seems likely from this work, it would help to eliminate mechanisms which rely on truly sudden onsets as plausible causes for glitching, such as sudden events involving the unpinning of vast numbers of superfluid vortices within the crust, triggered by mechanisms *other* than cracking in the solid crust.

Below we report (§2) on more than nearly nine years of observations of J0537, including more than four years of new observations, the whole of which argues that the time interval from one glitch (the first) to the next glitch (the second) in J0537 is strongly correlated to the amplitude of the first glitch (§3), a pattern that is similar to that of large quakes within the crust of our own planet. In §5 we compare the behavior of J0537 with that of the population of glitching pulsars and discuss how its glitch/time correlation helps to discriminate between different proposed mechanisms triggering their glitches. Section 6 lists our conclusions.

2. Observations

The data were obtained with the Proportional Counter Array (PCA) on board the RXTE observatory, as described in detail in M04. The PCA is sensitive to X-rays in the 2–60 keV band and has moderate spectral resolution ($\Delta E\ E^{-1} \sim 18\%$). Each event is time-tagged on the spacecraft with an uncertainty of less than 50 μs (Rots et al. 1998). The background consists of unrejected charged particles and X-rays from LMC X-1 and other cosmic X-ray sources. Only events in the first xenon layer in channels 5–50 ($\sim$3–20 keV) were included in this study. A log of RTXE observations of J0537 is given in Table 1. The observations are separated by 41 glitches into two incomplete and 40 complete groups. The number and epoch range for observations for which we have a timing solution (i.e., an unambiguous cycle count linking its pulse time of arrival [TOA] to those of at least one neighbor) are listed under "Phased," and the number and epoch range for the subset of these which were used to derive an ephemeris are listed under "Fit." Our monitoring system of J0537 continued as described in M04 except that, starting in late 2003 additional closely spaced observations were scheduled during the few week time period during which the next

glitch was anticipated.

3. Data Analysis and Results

3.1. The Pulse Profile

We first corrected the photon arrival events to the Solar System Barycenter using the source position (J2000) of $\alpha = 05^{hr}37^{m}47.36^{s}$, $\delta = -69°10'20.4''$ (Wang et al. 2001b). Times are given in barycentric dynamical time (TDB). Other details are as given in M04. For each observation we determined the pulsar's frequency and phase at the time of the first event (a nominal spindown, $\dot{\nu}$, of -1.988$\times10^{-10}$ Hz s^{-1} was used throughout these processes). The pulse shape was fitted at first to an ad hoc downward parabola with a half width at zero height of 0.072 cycles, but later to a master pulsar profile (MPP) derived from fitting folded data from many observations to a Breit-Wigner function (see, e.g., Nelson et al. 1970). The uncertainty in phase was determined from Monte Carlo simulations to be $\sim$0.04 S/N^{-1} cycles, where S/N is the signal-to-noise ratio of the single peak of the folded J0537 pulse profile, including noise fluctuations due to background and the pulsar signal itself. For the parameters of our observations (listed in M04) only about 0.5% of the count rate is due to the pulsar. However, these events account for six times as much variance per event than does the background, due to their concentration within the pulse profile shape.

Although several more iterations of this fitting made the next MPP sharper, eventually this process actually resulted in lower S/Ns, at least until we utilized the frequencies as derived from the timing solutions (see §3.2 below), which were much, much more accurate than could ever be achieved by fitting a single observation, to derive improved phases from a simple, one dimensional Newton-Raphson fitting process. The resulting MPP appeared to be wider at the top of the peak than any previously derived MPPs, and could no longer be well fit by any Breit-Wigner (BW) formula. Accordingly, we subtracted a Gaussian of a given center, narrow width, and small amplitude, from the BW formula, and this fit our first timing solution MPP well. Another MPP was generated by fitting to this modified BW (MBW), and this appeared to be flat at the top for at least 0.02 cycles. This master pulse profile and the MBW used to produce it are plotted in Figure 1.

Further iterations, with MPPs generated using the MBWs made by fitting to the MPPs from the previous iteration, could still be well fit by an MBW, but also produced MPPs that were progressively more "two-horned." These MBWs also produced progressively worse S/Ns when fit to the individual runs, a possible side effect of the interaction of statistics for the low S/N individual observations from which the MPP is produced, with the maximization

process for the fit response. The MPP drawn in Fig. 1 is given by:

$$L(\phi) = \frac{1-\phi(c_1-\phi c_2)}{1-\phi(c_3-\phi c_4)} e^{-c_5\phi^2}(1-c_6 e^{-c_7(\phi-\psi)^2}), \tag{1}$$

where $-0.5 \leq \phi \leq 0.5$. The three parameters that characterize individual runs were determined by fitting a function of the form $aL(\phi-\phi_0)+b$, where a gives the signal amplitude, b the background, and ϕ_0 defines the phase of the first pulse arrival in the observation time interval. A time of arrival (TOA) was obtained self-consistently by propagating the time of the first pulse peak arrival (derived from the measured pulse phase and the observation start time), by an integral number of cycles to some epoch near the center-of-gravity of the observation interval, using the nominal $\dot{\nu}$, together with the very accurate frequency given by the timing solution, or lacking that, the measured frequency for the individual observation. The constants, c_{1-7}, ψ, a, b, and ϕ_0 are given to full accuracy in Table 2. The phase, ϕ_0, like a and b, is in this case, for the MPP of Fig. 1, rather than any individual observation, and together with ψ, c_{1-7}, a, and b, makes a total of eleven parameters.

3.2. The Timing Solutions

The method of determining the timing solutions was the same as has been frequently employed for pulsars and other periodic phenomena. Per M04, the initial time gap between two observations (∼6–12 hours) was only a few times longer than the total time spanned by each observation, (5,000–20,000 s), usually consisting of 2–4 contiguously observed segments and their intervening gaps. This guaranteed that the average of the individual frequencies measured for two observations could reliably determine the mean frequency between the two. The time gap between the successive observations was then increased geometrically. A value for $\dot{\nu}$, close to those already determined from fits to other segments, or, lacking that, the long term frequency history of J0537, was used to count cycles over the longer time gaps. If the estimate of the number of cycles between TOA's from two consecutive observations was within a few hundredths of an integer, and the measured frequencies of the two observations were consistent with the same frequency and the small correction for $\dot{\nu}$, one could be confident that the cycle-counting was unambiguous.

Continued successes at cycle counting in extending the baseline of the timing solution quickly reduced the uncertainty of its validity to a vanishingly small value. When the time baseline of the observations and the gaps between them was sufficiently long, $\dot{\nu}$ could be reliably determined by the fitting process. Eventually, $\ddot{\nu}$ could be determined when the time baseline exceeded 100 days. The interval at which the gap size was reset to ∼6–12 hours was 60 days, and the whole timing procedure could be started over, if necessary. The cycle-

counting process was extended over a longer and longer time baseline, until a glitch made further extension of the unambiguous cycle-counting impossible.

A sum-squared minimizing routine was used to fit the data segments to a power law model, involving the pulsar braking index, n, in $\dot{\nu} \propto -\nu^n$. As an example, the frequency predicted by the power law relation at time t, can be, for the purposes of discussion, more conveniently expressed as:

$$\nu(t) = \nu(t_0)(1 - (\dot{\nu}(t_0)/\nu(t_0))(n-1)(t-t_0))^{-1/(n-1)}, \tag{2}$$

where t_0 is the epoch of the fit, and the quantity, $-\dot{\nu}(t_0)\nu(t_0)^{-1}$, is usually more concisely, though *not* as conveniently for the purposes of discussion, expressed as $\gamma(t_0)$. As a check on the power law parameters and their errors, ν, $\dot{\nu}$, and $\ddot{\nu}$, were derived, using simple linear algebra, from linear polynomial fits to the TOA's and cycle numbers of points belonging to the individual data segments:

$$m_i = \phi_0 + \nu(\mathrm{TOA}_i - t_0) + \dot{\nu}(\mathrm{TOA}_i - t_0)^2/2 + \ddot{\nu}(\mathrm{TOA}_i - t_0)^3/6, \tag{3}$$

where m_i is the integral number of cycles from time, t_0 - $\phi_0\nu^{-1}$ to TOA_i, ϕ_0 is the pulse phase at time, t_0, and the need for ϕ_0 can be eliminated by a proper choice of t_0. For another check, the power law fits were re-initialized with the equivalent parameters derived from the polynomial fits. The difference between the 3rd order polynomial fits using ν, $\dot{\nu}$, and $\ddot{\nu}$, and the power law fit that uses the equivalent parameters, consisting of terms of higher time derivatives than $\ddot{\nu}$, was insignificant.

In practice, when the data segments only contain a few points, they are first fit using only a fiducial phase or TOA, and ν, with $-\dot{\nu}\nu^{-1}$ and n fixed, then with only n fixed, and then with all four parameters. The parameters of the fits and their errors are listed in Table 3, along with an epoch of pulse peak arrival. In four cases of short data segments (5, 8, 13, and 17), and three segments with $\geq$100% errors on n (1, 6, and 11), n was fixed at 3.5 without much increase in chi-square. In three more segments (10, 14, and 20) with large errors on n and large chi-squared increases when n was set to 3.5, n was fixed at values near to what the four-parameter fit would have produced (31.5, 35.0 and 19.0). Of this last three, segment 14 showed evidence that the last point was high (see 3.4 and Figure 4). Segment 20 may have had both a small, but long-lasting recovery (the last and highest point of Segment 19 precedes it by only three days), and a later pre-glitch creep, as its favored braking index near 19 can only be diminished when observations were removed from near its beginning *and* its end, though more observation points would have been needed to be certain. This situation is likely to become more common as further segments with more near-glitch observations are obtained.

3.3. The Frequencies, and Spindowns

The errors on the frequency measurements of the individual observations were also calibrated by Monte Carlo simulations, and found to be [0.0418,0.045 cycles] (S/N T_{rms})$^{-1}$, for the upper and lower 1σ frequency errors, respectively. Here, T_{rms} is the square root of the mean squared moment in time for all of the events. For a continuous (i.e., unbroken) observation of duration T, T_{rms} is $(2\sqrt{3})^{-1}$ T, as long as the signal and background count rates don't change with time. A simple way to understand these errors is that the phase error is the half width at half maximum, 0.044 cycles (Fig. 1), divided by the S/N. The frequency error is then that error divided by T_{rms} (see, e.g., Ransom, Eikenberry, & Middleditch 2002). Figure 2 shows the individually measured frequencies of J0537 with a convenient $\dot{\nu}$ subtracted, along with the lines/curves representing the frequency trends from the timing solutions.

The first 40 of 41 glitches, ranging in size from 0.016 to 0.68 parts per million (ppm), are labeled in Fig. 2. The mean rate of decrease, -1.9760×10^{-10} Hz s^{-1}, is shown as the oblique dashed line. All of the comments on the behavior of the glitching made in M04 apply as well to this new total data set, now a factor of three times larger. The first glitch is still the largest of the 41, and a measurement of the braking index, n, characteristic of the actual physical mechanism which slows the rotation of J0537, appears to be as elusive as ever. However, the braking index of J0537 softens from 10.8 and 6.6 for the two halves of the long data segment 2, and there is some evidence for the same softening in most other long data intervals. For the moment though, it is impossible to know if this is inconsistent with the behavior of the high braking indices in non-glitching pulsars found by Johnston and Galloway (1999).

The history of $\dot{\nu}$ is shown in Figure 3. The points are derived from timing solutions of subsegments of data with at least three observations, spanning at least 1,400,000 s, and with at least one observation no further away from the span midpoint than 35% of the whole span. Observations were appended to the subsegments until these criteria were met. A slight exception was made for data segment 17 (hourglass at $\sim$ MJD 53,140), which only spans two weeks. Further observations from the end of the previous, fitted data subsegment were also prepended to the following subsegment when it would have otherwise spanned an insufficiently long time interval. An extra subsegment was generated at the end of data segments 7, 19, and 20 by sharing the last observation of the (otherwise) last subsegment.

Figure 3 shows the same strong trend of $\dot{\nu}$ recovery (the rapid change in $\dot{\nu}$, seen immediately after a glitch, which diminishes with time) as has been sketched in Fig. 4 of M04. Even in Fig. 2, the recovery of $\dot{\nu}$, in the long data section following the first glitch, is apparent as the decrease in the negative slope of the line representing the timing solution. The long

term trend, or steepening, from one line (timing solution frequency history) to those at later times, as first reported by M04, is also apparent in Fig. 2 by glitch 15.

Any slope, including those between the subsegment $\dot{\nu}$'s in Fig. 3, corresponds to a particular braking index n, as shown by the several dashed lines. The slopes are in general very high at the beginnings of the data segments, and in general diminish somewhat by the end of the data segments. The two parallel dotted lines are separated by 0.15 pHz s^{-1} and act as a guide for the changes of $\dot{\nu}$ within the data segments and the long term trend across all the data segments, which, at -0.15 pHz s^{-1} per five years, is an order of magnitude smaller (and opposite in sign) than the typical recovery trend of $\dot{\nu}$. Although the trends within the segments do not stay within the bounds delimited by the dotted lines, the *spans* of the $\dot{\nu}$'s within each segment are approximately equal. This will be discussed in further detail in section 3.6 below.

3.4. The Timing Solution Phase Residuals

The phase residuals for the timing fits to all of the data segments are shown in Figure 4, plotted as in M04, except that we have included the phase recoveries of the third and fourth data segments, and most of recovery of the seventh data segment. Doing this assures that the fits reflect the timing behavior of the pulsar during the segment as accurately as possible, and are best for measuring the changes in $\Delta\nu$ and $\Delta\dot{\nu}$ across the glitches (see §§3.5–3.6). As far we or anyone else can determine, such post-(large)-glitch recoveries in pulsars affect the timing in a continuous way, unlike the pre-glitch activity such as that seen for data segments 7, 12, 19, and 21, which will be discussed below. We have not plotted the 8 points[1] for which there is no timing solution.

Other timing irregularities are also apparent in a half dozen other data segments shown in Fig. 4, with both pre-glitch activity *and* a post-glitch recovery for data segment number 7 (circles) – the last and incomplete segment of M04 – and in six cases have been omitted from the timing fits, and so are flagged by filling in the hollow characters. Segment 7 is plotted with greater time resolution in Figure 5 (lower). Conservatively, at least the first point (filled circle) is part of a recovery from glitch 6, which, at 0.46 ppm (M04), is our third largest, and thus would have been expected if post- and pre-glitch activity scales with the size of the glitch. Data segment six contains an unphased observation as its last point, supporting this hypothesis. The points beyond MJD 52,150 are shown in the inset frame of Fig. 5.

[1]Note that one unphased point was plotted in both data segments 5 and 6, in Fig. 3 of M04 – the point belongs to data segment 5 as can be seen in Fig 2 herein.

In contrast, the microglitches at the end of data segments 12 and 21, plotted in Fig. 4 as filled squares and diamonds, are very well fit by $\Delta\nu$'s of 0.18 and 0.29 μHz, or gains in frequency of about three and five parts per billion (ppb). The duration of these features lasted for at least 16 and 11, and possibly as long as 30 and 18 days. This last interval continued, starting with an unphaseable observation at MJD 53,695 (the last unphased point at the end of segment 21 in Fig. 2), followed by a glitch before the beginning of the next segment at MJD 53,702. Both data segments 14 (Fig. 4: bowties) and 19 (elongated diamonds) have last points which are several sigma above the trend. Gaps of six and three days, respectively, follow these points.

In addition, segment 22 is also plotted in Fig. 5 (upper), and shows evidence for quasi-stable behavior in the form of a steadily increasing *rate* of "creep" in phase, broken by a *downward* glitch, before resuming an upward trend. The timing residuals for data segment 20 show more of a pure creep without the downward point (solid pentagons in Fig. 4). The creep can be considered as part of an exponentially increasing trend (see the Appendix), or as a slow creep of neutron superfluid vortices in the crust (Link, Epstein, & Baym 1993), or both. The downward glitch behavior is rare, but a similar event apparently occurred within data segment 1, removed in time from any glitch (Fig. 4, leftmost squares). It has now also occurred early in data segment 23 (Fig. 4, rightmost squares). We initially speculated that glitch 23, expected near 2006 August 7.8 UT, was going to be a large one, but a glitch of 1.12 μHz occurred around early UT August 4. The first four observations of this segment spanned 15.5 days, after which quasi-stable extended it by another 27.6 days, making the last point in Fig. 8 (upper) drop by nearly 30 days. Clearly a 1 μHz glitch is insufficient to settle this pulsar enough so that the tight correlation holds.

3.5. The Glitch Amplitude-Time to Next glitch Correlation

The glitches visible in Fig. 2 appear to have post-glitch, non-glitching time intervals which are highly correlated to their amplitudes. In order to test this correlation as accurately as possible, reliable measures of the glitch amplitudes and the time between glitches are desirable. We have chosen to use the frequencies of the two observation points just preceding and following the glitch, as evaluated/extrapolated by/from each of the two timing solutions from the whole data segments which preceded and followed the glitch, to determine the $\Delta\nu$ across the glitch. This procedure yields two pairs of frequencies, one pair for the pre-glitch point from each the two timing solutions, which yields the first estimate of $\Delta\nu$, and then another similar pair for the post-glitch point, which yields the second estimate of $\Delta\nu$, and the two estimates can be compared as a check. The agreement in all 40 (measurable so far)

cases is within a small fraction of one μHz. We then set the uncertainty on the time to the next glitch as a quarter of the sum of the gaps preceding and following the data segment between this glitch and the following. Thus half the entire time range possible for a glitch is given by $\pm$ one error, and the whole range by twice this.

Table 4 lists the glitch amplitudes determined as described above, while Figure 6 plots these amplitudes against the time interval to the next glitch,[2] for which the correlation coefficient is 0.94. The coefficient against the post-glitch stable time interval, i.e. the maximum time interval following the glitch when no glitches of any size are detected in the extrapolation of the timing solution (see the time interval correction in column seven of Table 4), is 0.96 due to improvements to the fit of glitches 2, 3, 5, 6, 8, 11–13, 15, 17, and 20, with all of these points plotted in Figure 7. Glitches 4, 9, 10, 14, 18, 21, and 22 were worse with the corrections, but only by small amounts each. By contrast, the scatter of the amplitudes against the time to the previous glitch, is random, with a correlation coefficient of 0.05.

Figure 8 shows the integral of the glitch amplitude with time. The upper frame plots the actual - predicted glitch times. The error bars are derived from the uncertainty in glitch onset times and, on the left hand vertical axis, are converted into an error in μHz through the slope of the oblique line drawn from the bottoms of glitch 1 to glitch 21 (but which was deliberately plotted offset by +10 days to allow easier comparison). The bottom frame of the figure shows occasional early glitching, such as the onset of glitch 3, which may persist early for several more glitches, evident as the match in slope between the lower corners and the oblique line. Eventually an episode, during which only small (ppb) glitches occur, extends the time range of the data segment prior to the next large glitch, thereby resetting the glitch clock mechanism closer to what it was prior to the previous (early) glitch. Data segments 7, 12, and 22, which follow glitches 6, 11, and 21, all of which end with quasi-stable behavior, appear to be such glitch-resetting segments. Considerable variation about this clock must still be possible, as glitches 13–17 alternate late and early onsets.

3.6. The Effect of Glitching on $\dot{\nu}$

The changes in $\dot{\nu}$ across the glitches, $\Delta\dot{\nu}$, and their errors, $\delta(\Delta\dot{\nu})$, were determined in a fashion similar to those for $\Delta\nu$, i.e., by forward and backward extrapolation of the timing solutions, and by evaluating $\dot{\nu}$ for the two observations bracketing the glitch in time. However, because the error in $\dot{\nu}$ is relatively much larger than that for ν, and depends

[2]We exclude from consideration the very small (ppb in frequency) timing irregularities at the ends of the data segments shown in Figs. 4 and 5

strongly on the epoch(s) chosen for the timing solutions, it is necessary to get $\Delta\dot{\nu}$ directly from the timing solutions, with epochs set to the times of the pair of observations which bracket each glitch (changing fit epochs was not necessary to measure the $\Delta\nu$'s). The errors for $\Delta\dot{\nu}$ listed in Table 4 are taken to be minimum of the two error estimates from each of these pairs.

The pattern of the glitch recovery in $\dot{\nu}$ shown in Fig. 3 indicates that the longer the interval which precedes any given glitch, the smaller the values of $|\dot{\nu}|$ and thus the larger the possible $|\Delta\dot{\nu}|$ across the glitch. However, as mentioned in §3.3, the post-glitch $|\dot{\nu}|$ does not seem to be able to differ from its pre-glitch counterpart by an indefinitely large amount. These two facts suggest that there may be a correlation between the change in $\dot{\nu}$ across the glitch and the time interval from the *previous* glitch, and that it might saturate for high values.

The $\Delta\dot{\nu}$'s listed in Table 4 (and plotted in Figure 9 against the duration of the previous intervals for 22 of the 41 glitches) are taken as the inverse-squared error mean of the two values of each pair, whose difference also serves as a check of this procedure. The largest difference between these two is 50 ppm (0.05 on the abscissa of Fig. 9) for glitch 11. The next largest difference, for glitches 10 and 16, is only 0.035 in Fig. 9, and all other differences are even smaller.

For glitches with $1,000\Delta\dot{\nu}\dot{\nu}^{-1} < 0.5$ (4, 5, 8, 10, 11, 13, & 17) the correlation coefficient is -0.88, while that for all glitches (2–22, excluding glitch 6 due to its large error) is only -0.77. By contrast, the correlation of $\Delta\dot{\nu}\dot{\nu}^{-1}$ with the interval to the following glitch is 0.12 (i.e., a negative correlation *against* the predominantly negative $\Delta\dot{\nu}$'s – the same as with the correlation of 0.12 for $\Delta\dot{\nu}$ vs $\Delta\nu$). However, as suspected, the truly remarkable result is the hard upper limit of 0.075% or 0.15 pHz s^{-1} for the change. The glitches near this limit, 2, 3, 7, 9, 15, 16, 18–21, and 22, all have relatively long previous intervals, bearing out the suspected correlation, as also does glitch 12. The correlation indicates that the interval which preceded the first glitch may not have been more than twice as long ($\sim$120 days) as the data segment for which observations have been taken, since the $\Delta\dot{\nu}$ across glitch 1 is 0.045%. It may also indicate that the true size of $\Delta\dot{\nu}\dot{\nu}^{-1}$ for glitch 14 was likely at the lower end of its error range, near 0.4, rather than near the symbol plotted at 0.56 or higher, in Fig. 9. Noticeable improvements (a few to several units or so) in the chi-squares of the runs achieved, e.g., by using the polynomial fit parameters to initialize a minimum sum-squares routine, will typically result in changes to $\Delta\dot{\nu}$ in Table 4 by only 1–2$\times10^{-14}$ Hz s^{-1}. However, in none of these cases did the $\Delta\dot{\nu}$ ever exceed 0.15 pHz s^{-1}.

4. Recapitulation

The observations of J0537 have revealed several unique and remarkable features "in need of explanation." The first is the tight correlation between the size of the glitches ($\Delta\nu$) with the time interval to the following glitch, with a slope of about 400 days ppm^{-1}. The correlation with the post-glitch stable time interval is even tighter. Second, the microglitches which precede the large glitches can be due to a simple small increment to the pulse frequency, ν, or an initially gradual, but more than linear change in frequency with time, or a combination of both. The data are also consistent with each glitch being followed by a smooth, but relatively small recovery involving the decay of only a few percent of the initial $\Delta\nu$.

Third, the long term trend of $|\dot{\nu}|$ with time is *increasing*, and thus the timing age of J0537, -0.5$\nu\dot{\nu}^{-1}$, continues to decrease at a rate of nearly one year per year. Another way of stating this is that the gain in $|\dot{\nu}|$ across the glitch, typically about 0.15 pHz s^{-1}, unlike the behavior of $\dot{\nu}$ in Vela noted by Alpar (1998), is not completely given back before the following glitch, with 10 percent of the gain remaining. Fourth, the change in $\dot{\nu}$, or $\Delta\dot{\nu}$, is correlated to the time interval to the *preceding* glitch, but clearly saturates at 0.15 pHz s^{-1}. And finally, the RXTE-band ($\sim$2–20 keV) pulse profile has only a single pulse with a flat maximum for at least 0.02 cycles, or 320 μs.

5. Discussion

In §5.1 we discuss the strong correlation between glitch size and the time to the next glitch, and explain how this helps in discriminating between current models applied to other glitching pulsars. To this we add a discussion of the change in spindown rate, $\Delta\dot{\nu}$, across and between the glitches in §5.2.1, and a brief discussion on glitch latency intervals in young pulsars in §5.2.2. The remaining longterm increase of $|\dot{\nu}|$, i.e., the increasing spindown with age, is then discussed in §5.2.3, including the possibility that the magnetic pole of J0537 is migrating away from its rotation axis, and the necessity for a glitch latency interval in the youth of J0537 similar to that observed in the present day young pulsars. Finally we finish this section with a brief discussion of the pulse profile, in §5.3.

5.1. The Glitch Size-Time to next Glitch Correlation

It is generally accepted by now that the moment of inertia contained by the neutron superfluid within the crust of an NS amounts to only about 1% of the total, which also includes

both that of the superfluid interior and the solid crust. Some glitches, including those of the Crab pulsar and B0540-69, may be "crustquakes," where the equilibrium configuration (EC) for the solid crust departs from its geometrical configuration as the pulsar spins down until eventually the crust cracks and settles.

Of course, settling of the crust alone can not possibly be responsible for all glitches in Vela, as the NS would run out of its supply of rotational oblateness after a few hundred years. Also, sufficient crust settling to produce a frequency change of only a fraction of a ppm, for a glitch in a low luminosity pulsar such as Vela, would involve the release of an easily observable amount of energy (likely in the soft X-ray band), which was not seen (Andersen & Ögelman 1995; Seward et al. 2000). In addition to the glitch models mentioned in this work, several alternative models for glitching in pulsars exist (see, e.g., the discussion and references in §6 of Dall'Osso et al. 2003). Other models have been proposed more recently (Chamel & Carter 2006; Jahan-Miri 2006a,b; Negi 2006; Peng, Luo, & Chou 2006; Zhou et al. 2004).

In glitching pulsars, the solid crust of the NS spins down continuously in between glitches, as the magnetic field is locked to it.[3] During this time at least part of the neutron superfluid within the crust is decoupled from its spindown, and thus becomes a second (and separate) stream. Thus, as the solid crust slows down, the vortex density of the second superfluid stream exceeds what would be appropriate for the solid crust (and the first superfluid stream) by an ever larger amount with time.

Andersson et al. (2004) have suggested that such a two-stream superfluid system is subject to an instability, analogous to the Kelvin-Helmholz instability, that acts when the difference in effective rotation rates between the two streams is greater than a certain amount, ω_{cr}. During a glitch this causes a transfer of at least part of the extra angular momentum in the second, and faster rotating superfluid stream, to the solid crust and the first superfluid stream within it, spinning up the pulsar by a certain rotational difference, $\Delta\nu$. Another view holds that an excess of vortices from "traps" located within the crust, transfer angular momentum to it when triggered by a variety of potential mechanisms, including crustquakes in addition to an ω_{cr} (see, e.g., Alpar 1998; Alpar et al. 1993; Epstein & Link 2000). We explore this issue further below.

The actual mean size of a glitch in J0537 after about 10^7 s (115.7 days) would only be about 18 μHz, or just over one day of spindown (see glitch 3 of Table 4), which is nearly exactly one hundred times smaller than the accumulated spindown over this time interval,

[3]Even now, it is not yet clear how or if the interior superfluid of the NS is coupled to the solid crust (Sedrakian & Sedrakian 1995; Andersson, Comer, & Prix 2004).

and thus supports the hypothesis of angular momentum transfer from an NS component with 1% of the moment of inertia (399.1 days per glitching ppm for J0537 mean that 0.9% of the spindown is being reversed by the glitching). For the Vela pulsar,[4] the glitches average 2.0 ppm, or 22 μHz, very close to the average glitch size for J0537, but this amounts to 17 days of spindown, or just over 1.5% of the accumulated spindown over the 2.8-year mean interval between its glitches, which again supports angular momentum transfer from a 1% NS component. The difference between 1.5–1.7% in Vela and 1% in J0537 may be due to the difference in their Q values,[5] as Wang et al. (2000) report 0.38 for the 1996 October 13th glitch.

The coincidence between the mean absolute glitch sizes for J0537 and Vela suggests that the neutron superfluid in the crusts of *all* NSs,[6] when triggered by some mechanism, which may not be the same for all pulsars, favor dumping some of, or even more than (in the case of finite Q), ω_{cr}. Relatively "large" glitches, amounting to gains of 32.4 and 28.0 μHz, still essentially within the range observed for both Vela and J0537, have also been observed from the 2 Hz PSR J1806-2125 (Hobbs et al. 2002) and the 4 Hz PSR J1614-5048 (Wang et al. 2000), respectively. Although these increases in spin *frequency* are the same to within a factor of 2, the corresponding increases in energy span more than an order of magnitude, which lends yet more support for the storage and exchange of *angular momentum* by vortices in the neutron superfluid which is thought to lie within the crust.

Although glitch 1 of J0537, at 42.2 μHz, is the largest glitch ever observed, the 34.5 and 34.3 μHz Vela glitches of 1978, July 13, and 2000, Jan. 16 come in a close second and third, matching the 34.2 μHz mid-March 2010 glitch of J0537, followed by the 32.4 μHz glitch from PSR J1806-2125 as a very close fourth. All known glitches with $\Delta\nu > 5$ μHz, are listed[7] in Table 5, and histogrammed in Figure 10, which shows a clear maximum size for all glitches of 40 μHz. This lends further support for an ω_{cr}, between the solid crust and part of the superfluid contained within it, and this maximum can not be much bigger than 40μHz$\times$100, or 4 mHz, i.e., one "revolution" every 250 s (Anderson & Itoh 1975). This would correspond to 8 years of spindown for Vela, but only about 8 months for J0537.

---

[4]Lyne et al. [2000] report 1.7% for most pulsars.

[5]Q is the fraction of the $\Delta\nu$ gained across a glitch which decays afterward.

[6]The existence of a maximum in $\Delta\nu$ for the crustal neutron superfluid also implies that the glitch of AXS J161730-505505 reported by Torii et al. (2000) likely occurred closer to MJD 50,600 and had an amplitude near 26.2 μHz, instead of between MJD 49,300 and MJD 50,000, when its amplitude would have had to have been between 42 and 115 μHz. We note that the timing age of AXS J161730-505505 is 16,000 years.

[7]Zavlin, Pavlov, and Sanwal (2004) report three possible glitches in the 424 ms pulsar, 1E1207-5209, all with likely $\Delta\nu$'s > 5 μHz, but other interpretations for the timing irregularities also exist.

The NS crust in Vela is nowhere near as stressed even after its 2.8-year mean inter-(large)glitch time interval than it is in J0537 after only four months. Specifically, the crust of Vela would have had to mostly settle by only 0.007 cm after 2.8 years, whereas the crust of J0537 would have had to mostly settle 0.06 cm in four months, as the settling distance, δR, where R is the radius of the neutron star and is assumed to be 12 km,[8] scales as $\nu\dot{\nu}$. The factor of 70 difference in crust settling rates between the two may mean that less than one large Vela glitch in 15 is initiated by crust cracking. After J0537 and the Crab, the glitching pulsar with the next highest $\dot{\nu}\nu$ (down by a factor of 18) is the 15 Hz J0205+6449. The pulsar with the lowest $\dot{\nu}\nu$ (down by a factor of 12,000) is the 2 Hz J1806-2125, but its $\dot{\nu}$ is down only by a factor of 200. Clearly most glitches in most pulsars can not be triggered by crust cracking; many of those in the Crab and B0540, and almost all of those in J0537 likely are.[9]

Since the large glitches in J0537 are probably initiated by crust cracking events, the extreme linearity in its glitch size-post glitch quiet timing interval could be due to the steady divergence of rotation rates, ν_1 and ν_2, of the two superfluid streams, and crust cracking occurring much more frequently than its large glitches,[10] which only triggers them when $\nu_2 - \nu_1 > \omega_{cr}$. The alternative, of having the amount of angular momentum dumped from many vortex traps proportional to the amount of settling in its solid crust, is harder to justify, as many vortex traps with differing saturations would result in a chaotic glitch-time relationship. The crust settling in J0537 would have to be a global, rather than a local event, dumping the vast majority of traps to the same level, which seems unlikely.

Another alternative would be to have just one trap (Franco et al. 2000; Jones 2002), but the pre-(large)glitch microglitches visible in Figs. 4 and 5 contraindicate this alternative. The

---

[8]The mean settling rate [drop/time] goes as $4\pi^2\dot{\nu}\nu\mathrm{R}^4$ (GM)$^{-1}$, and thus would double for R = 14 km.

[9]J0537 is so bright in most of the X-ray band, however, that the excess luminosity due to its crust settling might easily escape notice. Assuming, in the case of J0537, some 10^7 s worth of spindown causes the settling of a 1.2×10^6 cm radius by 0.054 cm and a glitch of 17.8 μHz, the specific energy gained from the gravitational field of 1.3×10^{14} cm s^{-2} would be 7×10^{12} ergs/gm. Using a specific heat estimate equal to that of water, or 4.17×10^7 ergs gm^{-1} K^{-1}, gives a temperature rise of 14.5 eV. The temperature rise for J0537's biggest glitch would be 34.5 eV. With an NS surface temperature of 80 eV, these rises might not be detectable, unless the specific heat is overestimated by a large factor. Link and Epstein (1996) have argued that such a medium deposition of energy within the NS crust could have caused the large glitch seen in Vela during 1988, Dec. 24 (Lyne, Smith, & Pritchard 1992), and have also suggested the same mechanism for Crab glitches, the difference in magnitude being due to the temperatures of the two NS crusts, i.e., age. One large Vela glitch out of the dozen known is consistent with the >15:1 ratio estimated above. Unfortunately, no X-ray observations bracket the 1988 Vela glitch.

[10]The cracking event glitch rate in Vela then would be larger than 1 in 15.

relatively poor linearity observed in Vela glitches would then result from two-stream rotational differences significantly greater than ω_{cr} before cracking could trigger a glitch, leakage due to vortex currents in the inter-glitch interval, or both. We note that a more complicated picture of the glitch processes within Vela is asymptotic to this linear relationship as the $\Delta\dot{\nu}$'s across its glitches become equal, which they very nearly are for the long term recovery components of the larger glitches of Vela (Alpar et al. 1993), certainly more so than for J0537.

Although it has been suggested that cracks play no role whatsoever in glitches (Jones 2003), the arguments are based on the difficulties of producing open cracks within the crust, while closed cracks are perfectly free to slide and grow, given sufficient stresses. The crust does have a certain mechanical strength, even with cracks, but this can not literally hold it up as it strains against gravity for any indefinite period of time as the stresses continue to increase. At stresses greater than the yield stress,[11] the solid crust may have a range of higher stresses wherein it undergoes plastic deformation (Ruderman 1991a,b,c; Ruderman et al. 1998). In this stage the crust will slowly dissipate most of the gravitational energy involved in its settling, and thus avoid a sudden, large *unobserved* release of gravitational energy during a glitch (from whatever settling is left over). The older a pulsar is, the more it has glitched in the past, and thus the more extensive the network of cracks is likely to be.

Eventually, for J0537, the stresses in the crust will exceed the stability criterion for a population of cracks which is always present, and these cracks then grow quickly in an unstable fashion (see, e.g., Dienes 1985 and references therein) until they relieve the stresses and subsequently stop growing, possibly coalescing into a fault which crosses the equator (Franco et al. 2000), and if $\nu_2 - \nu_1 > \omega_{cr}$, triggering a large glitch. It is also possible that, during this process, the cracks will network throughout the entire crust as they grow and intersect each other. The mechanics of cracks in solid materials, including the NS solid crust, is discussed further in the Appendix.

A glitch can occur slightly early if the previous glitch left cracks which were larger than those which usually occur, and these become unstable earlier (at lower stress levels), but would not cause a glitch which was too early because $\nu_2 - \nu_1 < \omega_{cr}$. In these cases the stress levels at which crack growth become unstable will be lower. A glitch could also occur later if the population of larger cracks is relatively depleted.

---

[11]For stresses below the yield stress, a solid body undergoes a strain which is strictly proportional to the applied stress, and this strain vanishes when the stress is removed. This is Hooke's Law for the elastic behavior of solids. At higher stresses the extra strain in the solid is permanent, and this is due to plasticity, crack growth, or a combination of both. Another strain component which can vanish when stresses are removed is due to crack opening.

5.2. The $\dot{\nu}$ Behavior

5.2.1. The $\Delta\dot{\nu}$ Behavior

We are still faced with the $\Delta\dot{\nu}$ across the glitches, its correlation with the interval *prior* to the glitch, the apparent saturation value of 0.15 pHz s^{-1}, and its long term increase in absolute value, in addition to the behavior of $\dot{\nu}$ between the glitches. If we consider that J0537, at 4,000 years of age, is a middle-aged pulsar which is much older than the Crab, and yet still less than half as old as Vela, the observed behavior of at least the $\dot{\nu}$ is what might be expected, at least empirically.

The glitches in the Crab pulsar (and in B0540) are sufficiently small and infrequent, with a dozen glitches with $\Delta\nu\nu^{-1}$ from 4×10^{-9} to 6×10^{-8} (Wong et al. 2001) between 1969 and 1999,[12] that they could only be due to a few vortex traps within the crust. Thus the excess angular momentum dumped into the crust when a glitch occurs in the Crab is small, and the glitch size is small (Alpar 1998; Alpar et al. 1994,1996).

In addition much of the gain in $\Delta\dot{\nu}\dot{\nu}^{-1}$ across its glitches, up to 4×10^{-4}, persists indefinitely, initially prompting some (Allen & Horvath 1997; Link & Epstein 1997; Link, Franco, & Epstein 1998; Ruderman et al. 1998) to attribute this to a gain in the magnetic dipole moment due to an increase in angle between the magnetic and rotation axes (see §5.2.3). However, the pulse profile of the Crab already has two peaks, and is thus hard to reconcile with pole migration. Perhaps a more likely possibility, as first suggested by Alpar et al. (1996), is that the initial crackup permanently destroys the ability of part of the Crab's solid crust to store vortices (creating "vortex depletion regions") thus reducing its effective moment of inertia, which, for a constant braking torque, leads to a permanent increase in spindown. On the other hand, Ruderman (2005) attributes this effect to a permanent change of braking torque across the glitch due to an increase of the component of the dipole moment perpendicular to the rotation axis, which, in turn, is caused by migration of magnetic flux tubes and vortices, rather than to any physical migration of the crust along the NS surface.

In the much older (wrt the Crab) Vela pulsar, the NS solid crust may be saturated

---

[12]Although the 1969 glitch of the Crab (MJD 40,493 – Boynton et al. 1969) is generally quoted as 4×10^{-9} in $\Delta\nu\nu^{-1}$, the observing coverage very near its time of occurrence was sparse, and there is good reason to believe that the actual $\Delta\nu\nu^{-1}$ was a full 10^{-8}. This is because a glitch was observed, in data taken by Rem Stone for J. E. Nelson and J. Middleditch, around 1 August, 1971 (very early in the [optical] observing season, which started earlier yet on 24 July), which was very accurately measured to be 4.2×10^{-9} in $\Delta\nu\nu^{-1}$. This glitch overlaid the 1969 glitch *nearly perfectly* when plotted on the same time scale but a different phase residual scale by a ratio of exactly 2:5. The timescale of an exponential decay of $\Delta\nu$ for this glitch, τ_c, was 2.4 days, in good agreement with $\tau_c = 3$ days reported by Wong et al. (2001) for its weaker glitches.

with cracks, allowing a considerable number of traps, and/or a substantial second superfluid stream, so that the excess angular momentum dumped into the solid crust during a glitch spins the whole star up by an average near 22 μHz every 2.8 years. The extra $\Delta\dot{\nu}\dot{\nu}^{-1}$ gained across its glitches, 4–7$\times10^{-3}$, appears to completely die away in a what seems to be a linear fashion (i.e. with constant braking index) through vortex currents (Alpar 1998), and the subsequent glitch is primed to occur when this process finishes. For Vela this means there's also a strong correlation between $\Delta\dot{\nu}$ across a glitch and the time to the next glitch, in addition to the same correlation for $\Delta\nu$ (Alpar et al. 1993).

The situation for J0537 differs either because the crust frequently doesn't wait for currents to finish giving away all of the gain in $|\Delta\dot{\nu}|$ before causing a glitch, or because of an increase in the strength of the magnetic field, or a small, permanent gain caused by realignment of the NS magnetic moment, or any combination of these. This does not require that the vortex currents in J0537 and Vela differ in any fundamental way, as the $|\Delta\dot{\nu}|$ gained from the glitch in J0537 subsequent to the early "giveaway" glitch is usually correspondingly more modest, as can be seen in Fig. 3.

Although the glitches of the adolescent pulsar, J0537, average about six times smaller than those of Vela in $\Delta\nu\nu^{-1}$, they are an order of magnitude more frequent, so that its glitch activity parameter,[13] is 0.9 ppm yr^{-1} as compared to Vela's 0.7 ppm yr^{-1}, and at 0.1–0.7$\times10^{-6}$, they are still larger than those of the Crab by about one order of magnitude. About 90% of its gain in $\Delta\dot{\nu}\dot{\nu}^{-1}$ (as opposed to 100% in Vela), of up to 7.5$\times10^{-4}$ (about an order of magnitude smaller than the relative gains in Vela) "decays away" prior to the next glitch, the only other difference from Vela being the softening of the J0537 braking index between its glitches. Since the absolute size of the glitches in J0537 are just as large, and in one case larger than those in Vela, the crust of J0537 is likely just as saturated with cracks as Vela. This may be more of a reflection of enhanced crust settling in J0537 due to its history of higher spin rates, than it is of actual age.

However, the relative amount of the gain in $\Delta\nu\nu^{-1}$ across a glitch in Vela that decays away afterward, or Q, at 0.38 (Wang et al. 2000) is about an order of magnitude larger than in J0537. The integrated extra spindown due to a typical glitch of J0537 of size ξ ppm, with a linear $\Delta\dot{\nu}$ recovery of 0.21 ξ pHz s^{-1} over the 400 ξ days until the next glitch, would slowly remove 0.059 ξ^2 ppm from the gain in ν across the glitch, during the interval to the next glitch, which is consistent with the barely visible recovery following glitch 1 shown in Fig. 2.

This decay may be caused by vortex currents from the interior superfluid to that in

[13]The glitch activity parameter is defined as: $A_g = \Sigma\Delta\nu_g/\nu/\Delta t$, where $\Sigma\Delta\nu_g$ is the sum of all spin frequency gains to ν from glitches, over a timespan, Δt.

the crust, during the interval following a glitch, which makes up for an *excess* of vortices dumped from traps and/or a second superfluid during the glitch. Interestingly, the agreement between the maximum values of the $\Delta\dot{\nu}$ of 0.15 pHz s^{-1} involved in the long term recovery following the glitches of Vela, J0537, *and* the Crab (the 1989 July 13 glitch – Wong, Backer, & Lyne 2001) is nearly perfect, even better than that of the maximum values of $\Delta\nu$ among all pulsars. This is what would be expected from one NS to the next, as crusts, vortex currents and moments of inertia are basically the same, perturbed possibly only by spin rate, magnetic field, and differences in mass and temperature.

5.2.2. Young Pulsars and the Latent Interval

Livingstone, Kaspi, and Gavriil (2005) have called attention to the two orders magnitude difference in the glitch activity parameter, between the Crab pulsar and B0540, as evidence for significant differences in the internal structure of neutron stars. Although the most obvious difference between these two is that between their pulse profiles, the harmonic content of B0540 (Seward, Harnden, & Helfand 1984; Middleditch & Pennypacker 1985) is similar to the optical pulse profile of Vela (Wallace et al. 1977), and distinct inclinations for the two sources could easily account for the rest. It is more likely that young pulsars such as the Crab, B0540, and B1509-58 don't glitch very frequently at first, having to rely on settling of their crusts in order to form their initial cracks (generating vortex depletion regions and vortex traps and/or more second superfluid domain in the process), which then help in the further crackup of the NS crust. In this case, the crustquake rate would increase exponentially (at least initially), with the product, $\dot{\nu}\nu$, and the age of the pulsar, τ:

$$\nu A_g \sim \ exp\ (\frac{\tau}{\Upsilon}\ \dot{\nu}\nu/(\dot{\nu}\nu)_{Crab}) \tag{4}$$

where Υ is an e-folding timescale of glitch activity. If we use the timing age of the pulsar, -0.5$\nu\dot{\nu}^{-1}$, in place of τ, then equation 4 becomes:

$$\nu A_g \propto \ exp\ (-\nu^2/(2\Upsilon(\dot{\nu}\nu)_{Crab})\ ), \tag{5}$$

and the e-folding time for B0540 would be three times as long as that of the Crab, due to its product, $\dot{\nu}\nu$, being three times smaller than that of the Crab, plus 25% because the timing age, τ, of B0540 (1,550 years) is 25% longer than that of the Crab (1,240 years).

The absolute glitch activity, $\Sigma\Delta\nu_g/\Delta t$, for B0540 is really 75 times less[14] than that of the Crab, but this can be made up if Υ = 170 years. For B1509, with a 6.6 Hz spin, a

[14]The Crab's νA_g is taken from Livingstone et al. (2005) to be 0.3 μHz yr^{-1}, whereas that of B0540 is 0.004 μHz yr^{-1}.

6.7×10^{-11} Hz s^{-1} spindown, and a 1,670 year timing age, its νA_g is only 28% of that of B0540, consistent with no glitches having been observed to date from B1509, both pulsars having been discovered in the early 1980s. If no starquake is observed from B1509 in the next few decades, then perhaps equation 4 will need a pre-exponential factor of $\dot{\nu}$, which is certainly needed for the glitching rate of mature pulsars like J0537 and Vela.

This is a simpler model than that employed by Alpar and Baykal (1994). The starquake rate must turn over and flatten out if the νA_g predicted for J0537 is to match the actual value of 56 μHz yr^{-1}, i.e., only a factor of 187 higher than that of the Crab. This νA_g is only a factor of 7 more than that of Vela, as compared to the factor of 12.5 expected from the ratio of their $\dot{\nu}$'s, both pulsars being old enough so that their cracking growth functions may have reached the same high constant value. This discrepancy is not serious and can be completely resolved if the Q in Vela is about 0.46, a value close to that measured by some, or if Vela is old enough to have a higher value of the cracking growth function than that of J0537, or a combination of both.

5.2.3. Magnetic Pole Migration

Three facts support J0537 as being born, and possibly still remaining, close to an aligned rotator: the singly-peaked pulse profile; the low value of its $\dot{\nu}$ with respect to that of the Crab pulsar,[15] which has almost twice the $\dot{\nu}$ and less than half the ν; and the long term increase of its $|\dot{\nu}|$. The increase in the magnitude of the (negative) $\dot{\nu}$ amounts to about 0.15 pHz s^{-1} every five years, or 0.95×10^{-21} Hz s^{-2}, but is still uncertain by about 25%. Settling of the NS over this time period due to spindown will produce a 0.1% reduction in the 8.4 m NS equatorial, centrifugal bulge, or 0.84 cm, and a change in the dipole moment due to scale size changes a thousand times smaller, if any at all because the magnetic axis is not close to either the rotational equator or pole.

If the *entire* stellar moment of inertia can drop by 0.1% over five years, then, provided the braking torque doesn't change, this could account for the 0.075% increase in $|\dot{\nu}|$ in the same period. However, if the effective magnetic dipole moment of the NS also drops, the

[15]Although the two pulsars have identical spindown luminosities ($-2\pi^2 I\nu\dot{\nu}$) of 5×10^{38} ergs s^{-1}, close to the Eddington luminosity for an NS, SN 1986J, which is now producing 200 times the luminosity of the Crab Nebula in the 2 cm band (Bietenholz, Bartel, & Rupen 2004), likely exceeds this in total luminosity by a large factor. Thus the spindown of J0537 is not smaller than that of the Crab because its spindown luminosity, and that of all pulsars, L_{sd}, is not likely to be limited to L_{edd}, even by processes which we do not yet fully understand. We also note that Shukre, Manchester, and Allen (1983) have suggested that the SS 433 binary system contains an aligned, rotating, accreting NS.

reduced braking torque could cancel the effect, but if it increases, it could help produce it (see, e.g., Ruderman 2005). If this effect is real in J0537, then it is because its has the highest product, $|\dot{\nu}\nu|$ of 1.2×10^{-8} Hz^2 s^{-1}. However, the same product for the Crab pulsar, 1.1×10^{-8} Hz^2 s^{-1}, is a close 2nd, and the Crab clearly has a robust, positive $\ddot{\nu}$ of 1.2×10^{-20} Hz s^{-2}. Still, some have suggested that the intrinsic magnetic fields of pulsars may increase with time (see, e.g., Blandford, Applegate, & Hernquist 1983), though until now, there has been little evidence to support this assertion (Wakatsuki et al. 1992), and the magnetic field of the NS remnant of SN 1986J is clearly very strong after only 20 years (Bietenholz et al. 2004). The effect in J0537 is consistent with a growth in its magnetic field of 0.375×10^{-4} yr^{-1}, or 35 MG yr^{-1}.

There remains only the migration of the magnetic axis as the possible cause of the long term increase of $|\dot{\nu}|$. As mentioned in the previous section, some have initially argued that the persistent spindown gains in the Crab pulsar following its glitches are not caused by pole migration (see, e.g., Link, Epstein, & Baym 1992), but instead by the formation of new vortex depletion regions, (Alpar et al. 1996). However, this only works for young pulsars which haven't glitched at the high rates that Vela and certainly J0537 have for many thousands of years.

Following arguments similar to those made previously by others (Allen & Horvath 1997; Link & Epstein 1997), and assuming that the spindown of J0537 is proportional to the effective magnetic moment, $|\underline{\mathrm{m}}_{eff}| = |\underline{\mathrm{m}} \times \underline{\nu}||\,\underline{\nu}|^{-1}$, squared, or $|\underline{\mathrm{m}}_{eff}|^2$, and that this quantity is in turn proportional to $\sin^2\alpha$, where α is the polar angle of $\underline{\mathrm{m}}_{eff}$ from the rotation axis, and is also a linear function of time, we have:

$$\alpha(t) = \dot{\alpha}t + \alpha_0, \tag{6}$$

$$\dot{\nu} = \beta \sin^2\alpha(t)\ (\frac{\nu(t)}{\nu_{psr}})^n, \tag{7}$$

$$\beta \sin^2\alpha(\tau_{psr}) = -2\times10^{-10}\ \mathrm{Hz\ s^{-1}}, \tag{8}$$

where n is the braking index (for now assumed to be 2.5 – the same as is characteristic for the Crab pulsar), $\dot{\alpha}$ is the time derivative of $\alpha(t)$, τ_{psr} is the age of J0537, α_0 is the initial value of $\alpha(t)$ for time 0, or $-\tau_{psr}$ from the present, and β is a negative constant with dimensions of $\dot{\nu}$. As the magnetic pole migrates away from the rotation axis, the increase in the effective magnetic moment produces the increase of the spindown as a function of time that is evident in Fig. 3. Thus the time derivative of equation 7 is equal to the long term trend seen in Fig. 3:

$$\ddot{\nu} = 2\dot{\alpha}\beta\sin\alpha(\tau_{psr})\cos\alpha(\tau_{psr}) + n\dot{\nu}_{psr}\beta\sin^2\alpha(\tau_{psr})/\nu_{psr} = -0.95\times10^{-21}\ \mathrm{Hz\ s^{-2}}. \tag{9}$$

We can remove the second term from the middle of equation 9 by subtracting an assumed known present day power law contribution, to $\ddot{\nu}$ for J0537, with $n = 2.5$, of $n\dot{\nu}_{psr}\beta \sin^2 \alpha(\tau_{psr})/\nu_{psr} = n\dot{\nu}_{psr}^2/\nu_{psr} = 1.6 \times 10^{-21}$ Hz s^{-2}, to get:

$$\ddot{\nu}_\alpha = 2\dot{\alpha}\beta \sin \alpha(\tau_{psr}) \cos \alpha(\tau_{psr}) = -2.55 \times 10^{-21} \text{ Hz s}^{-2}. \tag{10}$$

Dividing equation 8 by equation 10 to eliminate β gives:

$$\frac{\tan \alpha(\tau_{psr})}{2\dot{\alpha}} = 7.8 \times 10^{10} \text{ s, or } 2,475 \text{ years}, \tag{11}$$

a transcendental equation which can be solved for $\dot{\alpha}$, with $\alpha(t)$ as the simple linear function of time given in equation 6, and if α_0 and τ_{psr} are known.[16] Values for $\dot{\alpha}$ and α_0 which make $\alpha(\tau_{psr})$ exceed 90 degrees are naturally excluded. We can integrate equation 7 to extrapolate backward and forward to solve for $\nu(t)$ and $\dot{\nu}(t)$.

Since the absolute value of the tangent function is always greater than that of its argument, and $\dot{\alpha}$, and α_0 are, barring migration *toward* the rotation axis, positive, equation 11 indicates that the age of J0537, τ_{psr}, or at least, $\tau_\alpha \leq \tau_{psr}$, the duration for which there is a constant $\dot{\alpha}$, can not exceed 5,000 years. For reasonable values for α_0 and $\dot{\alpha}$ with $\tau_\alpha = 4{,}000$ years, equation 11 is a problem to solve. For example, with $\alpha_0 = 0.2$ radians, no value of $\dot{\alpha}$ exists that gets the left hand side of equation 11 below 3,368 years, as long as we assume τ_α = 4,000 years.

The magnetic pole migration rate, necessary to render equation 11 solvable, is plotted against its initial obliquity for various values of latency times, τ_{psr} - τ_α for $\tau_{psr} = 4{,}000$ years, in Figure 11 (lower). Four vertical lines for $\alpha_0 = 0.1$ to 0.4 radians, in steps of 0.1 radians, intersect the lower portions of the curves for 22 (believable) values of $\dot{\alpha}$. From equation 6 we have, for the present day magnetic obliquity, α_{psr}:

$$\alpha_{psr} = \dot{\alpha}\tau_\alpha + \alpha_0, \tag{12}$$

which we can rewrite for the duration of the active migrating interval, τ_α as:

$$\tau_\alpha = -\alpha_0/\dot{\alpha} + \alpha_{psr}/\dot{\alpha}. \tag{13}$$

Thus, given α_{psr} and $\dot{\alpha}$, the relation between α_0 and τ_α is a straight line with a slope of $-1/\dot{\alpha}$ and an intercept of $\alpha_{psr}/\dot{\alpha}$. This relation is plotted in the top frame of Fig. 11 for

[16]For a braking index, n, of only 2.0, near the lowest known established, glitch-free braking index for any young pulsar (Zhang et al. 2001; Cusumano, Massaro, & Mineo 2003; Livingstone et al. 2005), the right hand side of equation 11 increases to 2,830 years.

α_{psr} from 10 to 60 degrees in steps of 10 degrees, and illustrates those values of α_{psr} and α_0 which are necessary to keep the non-glitching interval believably small.

The time histories of ν(t) and $\dot{\nu}$(t), corresponding to the pairs of (α_0,$\dot{\alpha}$) from the lower frame of Fig. 11, are plotted in Figure 12. The figure shows a small range for the spin rate, ν, of J0537 at birth, between 75 and 80 Hz, and a much wider relative range for $\dot{\nu}$.

5.3. The Pulse Profile

The peak of the pulse profile of J0537 appears to be flat for at least 300 μs (Fig. 1). Following the line of argument from Golden et al. (2002) to test whether J0537 should be able to produce high energy pulsations, given a 0.02 cycle extent of the plateau, we determine that the magnetic field of the emitting region, B_{em} in Gauss is given by:

$$B_{em} = 10^{10} E, \tag{14}$$

where E is the energy of the peak of the pulsed synchrotron emission in keV. However, the Lorentz γ is only 8 from the same calculation, so it is hard to know if this analysis is appropriate for J0537. Assuming that it is, and extending a dipole field of 0.925 tG, and a radius of 12 km, gives 54 km for the location of pulsed keV emission. The field strength at a light cylinder with a 770 km radius would then be 3.5 MG, and thus J0537 would be expected to produce optical pulsations. However, if J0537 is a nearly-aligned rotator, the actual surface magnetic field may be near 3.5 tG, or higher. In that case the pulsed keV emitting radius moves out to 86 km, and the magnetic field at the light cylinder increases to 14 MG.

If the field does actually fall through 2–3 $\times 10^7$ G before reaching the light cylinder, by the logic of some (Cheng, Ho, & Ruderman 1986a,b), one might expect an outer gap region where pulsed optical emission could arise. Gil, Khechinashvili, and Melikidze (2001) model the pulsed optical emission from Geminga (Golden et al. 2002) assuming that, like J0537, it is a nearly aligned rotator. However, O'Connor, Golden, and Shearer (2005) argue that, in the case of J0537, its pulsed radiation is synchrotron self-absorbed at optical wavelengths, with $m_V \sim 24$. Unfortunately, the limits on optical pulsation are not very stringent, with the magnitude 23.4 limit from Mignani et al. (2000) derived from imaging alone and close to one solar luminosity, as compared to the Crab pulsar with 4 solar luminosities.

6. Conclusion

The 62 Hz pulsar in the LMC, J0537, is unique among all others. It is the fastest spinning young pulsar, and the most actively glitching pulsar known, with a gain in frequency of 56 μHz, as compared to Vela's 8 μHz, yr^{-1}. The extreme linearity of the glitch-size/post-glitch stable time, in addition to other quasi-stable behavior, is consistent with the crack growth mechanism in the NS solid crust for the initiation of its glitches, and a two superfluid stream instability within the solid crust, as the cause of the variation in glitch magnitude. Crack growth mechanisms may also cause glitching activity in young pulsars, such as the Crab and B0540, to increase exponentially with a 170-year timescale and the product, $\dot{\nu}\nu(\dot{\nu}\nu_{Crab})^{-1}$, and this may be detectable in the Crab after a few more decades. Among all pulsars, the important quantity involved in glitches is *angular momentum* transfer, i.e., $\Delta\nu$, rather than $\Delta\nu\nu^{-1}$ or $\nu\Delta\nu$, and 40 μHz appears to be an absolute maximum for this quantity. This represents an ω_{cr}, or a difference in rotation rate of one cycle per 250 s between the NS solid crust, and the superfluid vortices within it. The moment of inertia of the crustal superfluid is close 1% for J0537, lower than that ascribed to Vela and a few other pulsars, and the difference may explain why Q, the fraction of $\Delta\nu$ gained in the glitch which decays afterward, is an order of magnitude higher in these others.

The 62 Hz rotation frequency of J0537 is over twice that of the 30 Hz rate of the Crab pulsar, but yet its spindown rate is only slightly greater that half that of the Crab, and just barely larger than that of the 20 Hz rotator, PSR B0540-69. Clearly its effective magnetic dipole moment is only about 25% those of Vela, the Crab, and B0540. It may just have a weaker magnetic field than the others, but its singly-peaked pulse profile argues that, when it was born 4,000 years ago, it was as a nearly-aligned rotator, spinning at a rate between 75 and 80 Hz.

The longterm increase in the magnitude of its (negative) spindown, $|\ddot{\nu}|$, near 10^{-21} Hz s^{-2} (or 2.55×10^{-21} Hz s^{-2} after correcting for braking by magnetic dipole radiation and/or pulsar wind processes), supports the interpretation of magnetic pole migration away from the rotation axis over time, by about one radian every 10,000 years, or one meter on the NS surface per year, or even less. This rate agrees with the estimate, made in the Appendix, of the crack growth rate necessary to trigger the glitches in J0537. Like the Crab, or B0540, which, after 950 and 1,550 years, are both still in a low glitch-activity state, the interval of relatively low glitch activity in J0537 may have lasted 1,500 years, although realistic values for the initial obliquity and migration rate also exist for an interval as short as 400 years. The spindown rate, $|\dot{\nu}|$, for J0537 at birth was likely at least 30% less than it is today.

There also appears to be a maximum absolute value for the (almost always negative) change in spindown, $|\Delta\dot{\nu}|$, across (and for J0537 and Vela also equal to that involved in the

longterm recovery following), a glitch, in all pulsars, of 0.15 pHz s^{-1} (i.e., a *minimum* value of -0.15 pHz s^{-1}). This is equivalent to a maximum value for vortex currents within pulsars, though exactly how or why this occurs is still unknown. Finally, the single peak of the J0537 pulse profile is flat at its top for at least 0.02 cycles, or 320 μs.

J.M. thanks Drs. Ali Alpar, John Dienes, Aaron Golden, Naoki Itoh, David Pines, and Mal Ruderman for helpful, guiding conversations, and his group, CCS-3, for support during a substantial interval when he was without funding. E.V.G.'s research is supported by NASA grant NAG05GR11G. This research has made use of data obtained through the High Energy Astrophysics Science Archive Research Center Online Service, provided by the NASA/Goddard Space Flight Center. This research was performed in part under the auspices of the Department of Energy.

7. Appendix

From Dienes (1983) as corrected by Rice (1984), a penny-shaped crack will become unstable to rapid growth if the following inequality holds:[17]

$$(\sigma - \tau)^2 c > \frac{\pi}{2}\frac{2-\nu_p}{1-\nu_p}\gamma_{se}\mu, \tag{1}$$

where c is the crack radius, σ and τ are the traction and interfacial friction across the crack, ν_p is Poisson's ratio[18], γ_{se} is the specific surface energy (in, e.g., ergs cm^{-2}, or dynes cm^{-1}),[19] and μ is the shear modulus.[20] As the crack radius, c, increases, unstable growth will occur for lower stress levels.

Melting and "healing" of the cracks due to interfacial friction may also occur as their two surfaces slide against each other. Others may stop growing when they intersect neighboring cracks at a high angle ("T" cracks). Still others may rotate or translate within the solid

[17]Cracks in the shape of a disk lying in a plane are the only ones, aside from elliptical cracks, for which there is a known stress solution.

[18]A cylindrical rod of height, H, which undergoes a given small $\delta H H^{-1}$ when subjected to a uniaxial stress, will increase in radius by a $\delta R/R = \nu_p \delta H H^{-1}$. Poisson's ratio for an incompressible material is 0.5.

[19]The γ_{se} for water is 77 ergs cm^{-2}. Most familiar solid materials have γ_{se}'s well into the thousands. However, the γ_{se} for HMX crystals is only 50!

[20]If a solid body of height, H, is subjected to a small shear stress in an orthogonal direction to H by a pressure of P dynes cm^{-2}, and shears by δL in that direction, then its shear modulus, $\mu = PH(\delta L)^{-1}$.

crust so that the traction stress is reduced across the largest and hence, most unstable cracks, and others yet may disappear through subduction below the crust (Ruderman 1991a). As occurs with faults in the Earth's crust (see, e.g., Scholz 2002), the crack intersections in the NS crust and other local variations prevent the crustquake process from relieving *all* strains necessary for it to settle to its current EC.

As stated in the main text, data segments 7, 12, and 21, which may restore the "original" glitch timing shown in Fig. 8, all have a period of quasi-stable behavior during this interval, instead of a prompt (large) glitch. This behavior can be physically interpreted as the NS still having the "guilty" cracks which caused the onset of the previous glitch, except that these have been partially "repaired" by melting or some other mode of fusion for closed cracks. The repair process leaves the crack radius smaller, thus revising the failure stress upward toward the nominal value. As mentioned above, another possibility is rotation or translation of the crack over several consecutive glitch intervals until the traction stress at the time of early onset is no longer sufficient to cause the crack to grow in an unstable manner.

For the cases such as the end of data segments 20 and 22 (Figs. 4 and 5) which shows a very gradual onset of angular momentum transfer, it is necessary to show that crack growth can have a gradual, slow rise in velocity from zero, or a "creep" phase. Evans (1974) and Charles (1958) have observed that, when the stress is below the critical level of instability given above in Equation (1), cracks may grow at low speeds:

$$v = v_R (K/K_1)^k, \tag{2}$$

where v is the crack growth speed, v_R is the Rayleigh velocity, $0.93\sqrt{\mu\rho^{-1}}$, the speed of a surface (shear) wave in the material of density, ρ, K is the stress intensity factor at the crack tip, $\sqrt{\pi c}(\sigma - \tau)$, K_1 is some stress intensity scale factor, and the optimum k is 12 for many brittle materials. The gradual behavior observed in data segments 20 and 22 (Fig. 5) may be the result of such a process. This formula holds only for a stress intensity factor, K, below a certain critical value, $K_0 = \sqrt{2\pi E \gamma_{se}}$, where E is Young's Modulus[21], and γ_{se} again, is the specific surface energy. For higher stress concentration factors, Freund (1990) has shown in theoretical studies that:

$$v = v_R (1 - (K_0/K)^2), \tag{3}$$

and this equation may likely govern the crack speed behavior for all sudden glitches. A value for the scale of the stress concentration factor, K_1, can be derived by setting the values and

[21] A body of length, L, when subjected to a small tensile force per unit area, σ, will strain by an amount, $\delta L = \sigma L E^{-1}$, where E is the Young's Modulus (and δL will drop to 0 when $\sigma = 0$). The shear modulus, μ is related to E and Poisson's ratio, ν_P, by $E = 2\mu(1 + \nu_P)$.

slopes of the v's for the two regions equal:

$$K_1 = K_0(k/2)^{1/k}(1+2/k)^{1/2+1/k}. \tag{4}$$

From equation 1, the critical radius for closed penny-shaped cracks is:

$$c_{cr} = \frac{\pi}{2}\frac{(2-\nu_P)}{(1-\nu_P)}\frac{\gamma_{se}\mu}{(\sigma-\tau)^2}, \tag{5}$$

and the corresponding fracture toughness is then:

$$K_0 = \sqrt{\pi c_{cr}}(\sigma-\tau) = \pi\sqrt{(1-\nu/2)\gamma_{se}\mu(1-\nu)}. \tag{6}$$

And finally, the relative crack speed at which the two stress concentration factors are equal is:

$$v/v_R = 1/(1+k/2), \tag{7}$$

which is 1/7 for $k = 12$.

We can estimate[22] the critical crack radius from equation 5 by taking $\mu = 2\times10^{29}$ dynes cm^{-2} from Ruderman (1991b), the values for the displacement field near 0.05 cm from Baym and Pines (1971 – also as equations 1 & 2 in Link et al. 1998), a $\nu_P = 0.5$ for incompressible matter, and amortizing this displacement over 1 km of crust to get a strain near 5×10^{-7}. Using the strain times a Young's modulus of $3\mu = 6\times10^{29}$ dynes cm^{-2}, yields a stress of 3×10^{23} dynes cm^{-2}, or 3×10^{14} kBar, reassuringly close to yield stresses for normal, everyday metals scaled up to NS mid-crustal densities. For a realistic γ_{se}, we can scale up 10^4 ergs cm^{-2}, for a material with a mean density of 5, by 1×10^{13} to match the density of the outer crust, and we can ignore, for the moment, the interfacial friction, τ. Using equation 5 the resulting critical crack radius, for the onset of instability for these (hypothetical) conditions in the crust, is $c_{cr} = 5.5$ cm. Of course this value will increase for any non-zero value for the interfacial friction, with a τ of half of the 3×10^{14} kBar stress given above increasing c_{cr} to 22 cm. Thus the total growth needed per year for the glitches then approaches one meter, in agreement with the amount of pole migration required to account for the persistent increasing trend in $|\dot{\nu}|$.

The crust will also have some distribution of crack sizes, as occurs in the Earth's crust, which is exponential over many orders of magnitude (Scholz 2002). In this case, there will be some probability that a crack of a certain size exceeding some limit will be present in the volume of interest. If the volume is not large enough, then there might well be no crack larger than that limit, and thus statistics enter into calculations of NS crust failure, just as it does in calculations of mechanical failure for other solid materials.

[22]Or calculate, as is done in Strohmayer et al. (1991)

REFERENCES

Allen, M. P., & Horvath, J. E. 1997, MNRAS, 287, 615

Alpar, M. A. 1998, in The Many Faces of Neutron Stars, Proc. NATO ASI – Lipari, Italy, eds. R. Buccheri, J. van Paradijs & M.A. Alpar, (Dordrecht: Kluwer), 59

Alpar, M. A., & Baykal, A. 1994, MNRAS, 269, 849

Alpar, M. A., Chau, H. F., Cheng, K. S., & Pines, D. 1993, ApJ, 409, 345

Alpar, M. A., Chau, H. F., Cheng, K. S., & Pines, D. 1994, ApJ, 427, L29

Alpar, M. A., Chau, H. F., Cheng, K. S., & Pines, D. 1996, ApJ, 459, 706

Andersen, D. R., & Ögelman, H. 1995, BAAS, 27, 880

Anderson, P. W., & Itoh, N. 1975, Nature, 256, 25

Andersson, N., Comer, G. L., & Prix, R. 2004, MNRAS, 354, 101

Arzoumanian, Z., Nice, D. J., Taylor, J. H., & Thorsett S. E. 1994, ApJ, 422, 671

Baym, G., & Pines, D. 1971, Ann. Phys., 66, 816

Bietenholz, M. F., Bartel, N., & Rupen, M. P. 2004, Science, 304, 1947

Blandford, R. D., Applegate, J. H., & Hernquist, L. 1983, MNRAS, 204, 1025

Boynton, P. E., Groth, E. J., Partridge, R. B., & Wilkinson, D. T. 1969, IAU Circ., No. 2179

Camilo, F., et al. 2004, ApJ, 611, L25

Chamel, N., & Carter, B. 2006, MNRAS, 368, 796

Charles, R. J. 1958, J. Appl. Physics, 29, 12, 1652

Cheng, K. S., Ho, C., & Ruderman, M. 1986a, ApJ, 300, 500

Cheng, K. S., Ho, C., & Ruderman, M. 1986b, ApJ, 300, 522

Cordes, J. M., Downs, G. S., & Krause-Polstorff, J. 1988, ApJ, 330, 847

Crawford, F., Kaspi, V. M., Manchester, R. N., Camilo, F., Lyne, A. G., & D'Amico, N. 1998, Mem. Soc. Astron. Italiana, 69, 951

Cusumano, G., Massaro, E., & Mineo, T. 2003, A&A, 402, 647

Dall'Osso, S., Israel, G. L., Stella, L., Possenti, A., & Perozzi, E. 2003, ApJ, 599, 485

Datta, B., & Alpar, M. A. 1993, A&A, 275, 210

Dienes, J. K. 1983, J. Geophys. Res., 88, 1173

Dienes, J. K. 1985, Mech. of Mat., 4, 325

Dodson, R. G., McCulloch, P. M., & Lewis, D. R. 2002, ApJ, 564, L85

Downs, G. S. 1981, ApJ, 249, 647

Epstein, R. I., & Link, B 2000, in Stellar Astrophysics, ed. L. S. Cheng et al. (Dordrecht:Kluwer), 95

Espinoza, C. M., Lyne, A. G., Stappers, B. W., & Kramer, M 2011, MNRAS, in press, arXiv:1102.1743

Evans, A. G. 1974, Int. J. Fracture, 10, 2, 251

Flanagan, C. S. 1990, Nature, 345, 416

Flanagan, C. S. 1991, IAU Circ., No. 5311

Flanagan, C. S. 1994a, IAU Circ., No. 6038

Flanagan, C. S. 1994b, IAU Circ., No. 6064

Flanagan, C. S., & Buchner 2006, CBET, No. 595

Franco, L., Link, B., & Epstein, R. I. 2000, ApJ, 543, 987

Freund, L. B. 1990, Dynamic Fracture Mechanics (Cambridge: Cambridge Univ. Press 1998)

Gil, J., Khechinashvili, D. G., & Melikidze, G. I. 2001, ApJ, 551, 867

Golden, A., Shearer, A., Redfern, R. M., Beskin, G. M., Neizvestny, S. I., Neustroev, V. L., Plokhotnichenko, V. L., & Cullum, M. 2002, A&A, 363, 617

Hessels, J. W., Roberts, M. S. E., Ransom, S. M., Kaspi, V. M., Romani, R. W., Ng, C.-Y., Freire, P. C. C., & Gaensler, B. M. 2004, ApJ, 612, 389

Hobbs, G., et al. 2002, MNRAS, 333, L7

Jahan-Miri, M. 2005, JLTP, 139, 373

Jahan-Miri, M. 2006, New A, 11, 157

Johnston, S., & Galloway, D. 1999, MNRAS, 306, L50

Johnston, S., Manchester, R. N., Lyne, A. G., Kaspi, V. M., & D'Amico, N. D. 1995, A&A, 293, 795

Jones, P. B. 2002, MNRAS, 335, 733

Jones, P. B. 2003, ApJ, 595, 342

Kaspi, V. M., Manchester, R. N., Johnston, S., Lyne, A. G., & D'Amico, N. D. 1992, ApJ, 399, L155

Krawczyk, A., Lyne, A. G., Gil, J. A., & Joshi, B. C. 2003, MNRAS, 340, 1087

Kuiper, L., Hermsen, W. 2009, A&A, 501, 1031

Link, B., & Epstein, R. I. 1996, ApJ, 457, 844

Link, B., & Epstein, R. I. 1997, ApJ, 478, L91

Link, B., Epstein, R. I., & Baym, G. 1992, ApJ, 390, L21

Link, B., Epstein, R. I., & Baym, G. 1993, ApJ, 403, 285

Link, B., Epstein, R. I., & Lattimer, J. M. 1999, Phys. Rev. Lett., 83, 3362

Link, B., Franco, L. M., & Epstein, R. I. 1998, ApJ, 508, 838

Livingstone, M. A., Kaspi, V. M., & Gavriil, F. P. 2005, ApJ, 633, 1095

Lyne, A. G. 1987, Nature, 326, 569

Lyne, A. G., Pritchard, R. S., & Smith, F. G. 1993, MNRAS, 265, 1003

Lyne, A. G., Shemar, S. L., & Smith, F. G. 2000, MNRAS, 315, 534

Lyne, A. G., Smith, F. G., & Pritchard, R. S. 1992, Nature, 359, 706

Manchester, R. N., Newton, L. M., Hamilton, P. A., & Goss, M. 1983, MNRAS, 202, 269

Marshall, F. E., Gotthelf, E. V., Middleditch, J., Wang, D. Q., & Zhang, W. 2004, ApJ, 603, 682 (M04)

Marshall, F. E., Gotthelf, E. V., Zhang, W., Middleditch, J., & Wang, Q. D. 1998, ApJ, 499, L179

McCulloch, P. M., Hamilton, P. M., McConnell, D., & King, E. A. 1990, Nature, 346, 822

McCulloch, P. M., Hamilton, P. M., Royle, G. W. R., & Manchester, R. N. 1983, Nature, 302, 319

McCulloch, P. M., Klekociuk, A. R., Hamilton, P. A., & Royle, G. W. R. 1987, Aus. J. Phys., 40, 725

Middleditch, J., et al. 2000, New A, 5, 243

Middleditch, J., & Pennypacker, C. R. 1985, Nature, 313, 159

Mignani, R. P., Pulone, L, Marconi, G., Iannicola, G., & Caraveo, P. A. 2000, A&A, 355, 603

Negi, P. S. 2006, MNRAS, 366, 73

Nelson, J., Hills, R., Cudaback, D., & Wampler, J. 1970, ApJ, 161, L235

O'Connor, P., Golden, A., & Shearer, A. 2005, ApJ, 631, 471

Peng, Q-H., Luo, Z.-Q., & Chou, C-K. 2006, Chinese J. Astron. Astrophys., 6, 297

Pines, D., & Alpar, M. 1985, Nature, 316, 27

Ransom, S., Camilo, F., Kaspi, V., Slane, P., Gaensler, B., Gotthelf, E., & Murray, S. 2004, in X-Ray Timing 2003: Rossi and Beyond, Proc. AIP – Cambridge, MA eds. P. Kaaret, F. K. Lamb, & J. H. Swank, 714, 350

Ransom, S. M., Eikenberry, S. S., & Middleditch, J. 2002, AJ, 124, 1788

Rice, J. R. 1984, J. Geophys. Res., 89, 2415

Rots, A. H., et al. 1998, ApJ, 501, 749

Ruderman, M. 1991a, ApJ, 366, 261

Ruderman, M. 1991b, ApJ, 382, 576

Ruderman, M. 1991c, ApJ, 382, 587

Ruderman, M. 2005, preprint (astro-ph/0510623)

Ruderman, M., Zhu, T., & Chen, K. 1998, ApJ, 492, 267

Scholz, C. H. 2002, The Mechanics of Earthquakes and Faulting, 2nd edition (Cambridge University Press: Cambridge)

Sedrakian, A. D., & Sedrakian, D. M. 1995, ApJ, 447, 305

Seward, F. D., Alpar, M. A., Flanagan, C., Kiziloĝlu, Ü., Markwardt, C., McCulloch, P., & Ögelman, H. 2000, ApJ, 536, 948

Seward, F. D., Harnden, F. R. Jr., & Helfand, D. J. 1984, ApJ, 287, L19

Shemar, S. L., & Lyne, A. G. 1996, MNRAS, 282, 677

Shukre, C., Manchester, R. N., & Allen, D. A. 1983, Nature, 303, 501

Strohmayer, T., Ogata, S., Iyetomi, H., & Ichimaru, S., & Van Horn, H. M. 1991, ApJ, 375, 679

Torii, K., Gotthelf, E. V., Vasisht, G., Dotani, T., & Kinugasa, K. 1999, ApJ, 534, L71

Urama, J. O., & Okeke, P. N. 1999, MNRAS, 310, 313

Urama, J. O. 2002, MNRAS, 330, 58

Wakatsuki, S., Hikita, A. , Sato, N., & Itoh, N. 1992, ApJ, 392, 628

Wallace, P. T., et al. 1977, Nature, 266, 692

Wang, N., Manchester, R. N., Pace, R. T., Bailes, M., Kaspi, V. M., Stappers, B. W., & Lyne, A. G. 2000, MNRAS, 317, 843

Wang, N., Manchester, R. N., Zhang, J., Wu, X. J., Yusup, A., Lyne, A. G., Cheng, K. S., & Chen, M. Z. 2001a, MNRAS, 328, 855

Wang, Q. D., & Gotthelf, E. V. 1998, ApJ, 494, 623

Wang, Q. D., Gotthelf, E. V., Chu, Y.-H., & Dickel, J. R. 2001b, ApJ, 559, 275

Wong, T., Backer, D. C., & Lyne, A. G. 2001, ApJ, 548, 447

Yuan, J. P., Manchester, R. N., Wang, N., Zhou, X., Liu, Z. Y., & Gao, Z. F. 2010, ApJ, 719, L111

Zavlin, V. E., Pavlov, G. G., & Sanwal, D. 2004, ApJ, 606, 444

Zhang, W., Marshall, F. E., Gotthelf, E. V., Middleditch, J., & Wang, Q. D. 2001, ApJ, 554, L177

Zhou, A. Z., Xu, R. X., Wu, X. J., & Wang, N. 2004, Astrop. Phys., 22, 73

This preprint was prepared with the AAS LaTeX macros v5.2.

Table 1. Observing Log

Segment Number	Total number of Observations	Start-End MJD-MJD	Number of Phased Observations	Start-End MJD-MJD	Number of fit Observations	Start–End[a] MJD - MJD
1	11	51197 - 51276	10	51197 - 51262	10	51197 - 51262
2	30	51294 - 51560	28	51310 - 51546	28	51310 - 51546
3	17	51576 - 51705	17	51576 - 51705	17	51576 - 51705
4	18	51715 - 51818	18	51715 - 51818	18	51715 - 51818
5	9	51833 - 51874	8	51833 - 51864	8	51833 - 51864
6	10	51886 - 51954	9	51886 - 51941	9	51886 - 51941
7	31	51964 - 52165	31	51964 - 52165	25	51973 - 52144
8	9	52175 - 52229	9	52175 - 52229	9	52175 - 52229
9	22	52252 - 52382	22	52252 - 52382	22	52252 - 52382
10	11	52389 - 52445	11	52389 - 52445	11	52389 - 52445
11	13	52460 - 52539	13	52460 - 52539	13	52460 - 52539
12	31	52551 - 52733	31	52551 - 52733	27	52551 - 52715
13	10	52745 - 52814	8	52745 - 52792	8	52745 - 52792
14	12	52822 - 52884	12	52822 - 52884	12	52822 - 52884
15	12	52889 - 53007	12	52889 - 53007	12	52889 - 53007
16	14	53019 - 53122	14	53019 - 53122	14	53019 - 53122
17	5	53128 - 53142	5	53128 - 53142	5	53128 - 53142
18	15	53147 - 53285	15	53147 - 53285	15	53147 - 53285
19	21	53290 - 53443	21	53290 - 53443	20	53291 - 53440
20	15	53446 - 53549	15	53446 - 53549	11	53446 - 53538

Table 1—Continued

Segment Number	Total number of Observations	Start-End MJD-MJD	Number of Phased Observations	Start-End MJD-MJD	Number of fit Observations	Start–End[a] MJD - MJD
21	20	53551 - 53696	20	53551 - 53696	16	53551 - 53682
22	19	53711 - 53859	19	53711 - 53859	14	53711 - 53839
23	13	53862 - 53950	13	53862 - 53950	10	53862 - 53933
24	8	53953 - 53996	8	53953 - 53996	4	53953 - 53968
25	11	54003 - 54099	11	54003 - 54099	10	54003 - 54088
26	23	54116 - 54273	23	54116 - 54273	17	54116 - 54252
27	17	54277 - 54441	17	54277 - 54441	17	54277 - 54441
28	13	54448 - 54534	13	54448 - 54534	11	54448 - 54527
29	6	54538 - 54573	6	54538 - 54573	6	54538 - 54573
30	11	54579 - 54634	11	54579 - 54634	11	54579 - 54634
31	17	54640 - 54710	17	54640 - 54710	17	54640 - 54710
32	10	54714 - 54767	10	54714 - 54767	10	54714 - 54767
33	13	54771 - 54885	13	54771 - 54885	13	54771 - 54885
34	14	54897 - 55027	14	54897 - 55027	14	54897 - 55027
35	25	55049 - 55182	25	55049 - 55182	9	55049 - 55122
36	14	55185 - 55263	14	55185 - 55263	14	55185 - 55263
37	17	55275 - 55444	17	55275 - 55444	17	55275 - 55444
38	7	55445 - 55516	7	55445 - 55516	7	55445 - 55516
39	8	55521 - 55549	8	55521 - 55549	8	55521 - 55549
40	7	55563 - 55584	7	55563 - 55584	7	55563 - 55584

Table 1—Continued

Segment Number	Total number of Observations	Start-End MJD-MJD	Number of Phased Observations	Start-End MJD-MJD	Number of fit Observations	Start–End[a] MJD - MJD
41	6	55589 - 55611	6	55589 - 55611	6	55563 - 55611
42	14	55619 - 55779	14	55619 - 55779	14	55619 - 55779

[a]Observations fit to determine the pulsar ephemerides given in Table 3.

Table 2. Master Pulse Profile (MPP)[a,b]

Constant Name	Value	
a	98,969.	6
b	1,791,946.	
ϕ_0	0.	5050471985806
ψ	0.	0104528014194
c_1	24.	51180526856
c_2	295.	1283580927
c_3	41.	89721595187
c_4	1,168.	592235964
c_5	111.	6330356226
c_6	0.	3315320354509
c_7	3,145.	824919010

[a] $L(\phi) = \frac{1-\phi(c_1-\phi c_2)}{1-\phi(c_3-\phi c_4)} e^{-c_5\phi^2}(1 - c_6 e^{-c_7(\phi-\psi)^2})$

[b] $MPP = aL(\phi - \phi_0) + b; \quad 0. \leq \phi \leq 1.0$

Table 3. Ephemerides for PSR J0537−6910

#	Epoch[a] (MJD)	ν (Hz)	$\dot{\nu}$ ($10^{-10} Hz\ s^{-1}$)	n	$\ddot{\nu}$ ($10^{-21} Hz\ s^{-2}$)	# fit	Reduced χ^2
1	51197.154619341040(14)	62.040931952(9)	-1.992409(17)	3.5[b]	2.2[b]	11	4.88
2	51423.704282859760(20)	62.037074298(2)	-1.992233(3)	6.9(1)	4.4(1)	31	4.20
3	51628.894751423615(35)	62.033570178(8)	-1.992751(17)	12.3(14)	7.9(9)	17	2.16
4	51738.867501147602(89)	62.031696343(30)	-1.993109(59)	18.4(46)	11.8(29)	18	1.60
5	51854.123449948998(9)	62.029720615(9)	-1.992993(75)	3.5[b]	2.2[b]	8	0.17
6	51911.260349119770(9)	62.028745439(4)	-1.992928(20)	3.5[b]	2.2[b]	9	3.25
7	51994.414099348115(162)	62.027341881(28)	-1.993125(28)	10.6(11)	6.8(7)	25	2.37
8	52209.375947238708(9)	62.023652330(4)	-1.993240(21)	3.5[b]	2.2[b]	9	1.26
9	52260.403693860565(305)	62.022799990(69)	-1.993398(92)	10.6(48)	6.8(31)	22	0.70
10	52415.443285215794(10)	62.020140505(3)	-1.993352(18)	31.5[b]	20.2[b]	11	1.06
11	52460.230974893198(13)	62.019382706(6)	-1.993317(10)	3.5[b]	2.2[b]	13	1.80
12	52570.946476496068(194)	62.017502072(34)	-1.993557(33)	11.0(13)	7.1(8)	27	1.37
13	52768.097565735862(11)	62.014115960(5)	-1.993603(32)	3.5[b]	2.2[b]	8	0.32
14	52823.911059168878(11)	62.013170456(8)	-1.994199(15)	35.0[b]	22.4[b]	12	1.29
15	52930.878736378858(51)	62.011342395(13)	-1.993621(28)	19.6(22)	12.6(14)	20	1.06
16	53038.548169014621(89)	62.009509017(34)	-1.993925(62)	15.0(42)	9.6(27)	14	1.35
17	53140.933489443908(16)	62.007746465(63)	-1.994542(641)	3.5[b]	2.2[b]	5	0.48
18	53155.874615682415(277)	62.007513323(65)	-1.994108(71)	13.2(32)	8.5(20)	15	2.21
19	53312.574782208428(163)	62.004838505(39)	-1.994275(44)	16.0(19)	10.2(12)	20	3.44
20	53450.087308030898(17)	62.002485827(6)	-1.994458(8)	19.0[b]	12.2[b]	11	0.84

Table 3—Continued

#	Epoch[a] (MJD)	ν (Hz)	$\dot{\nu}$ ($10^{-10} Hz\ s^{-1}$)	n	$\ddot{\nu}$ ($10^{-21} Hz\ s^{-2}$)	# fit	Reduced χ^2
21	53557.045117649134(573)	62.000663106(128)	-1.994517(133)	17.5(58)	11.2(37)	16	1.49
22	53812.224921513890(233)	61.996292178(70)	-1.993782(100)	12.7(58)	8.1(37)	14	0.60
23	53881.096858706792(13)	61.995120229(6)	-1.994542(17)	15.0[b]	9.6[b]	10	2.56
24	53952.688114056294(26)	61.993888026(61)	-1.995140(443)	15.0[b]	9.6[b]	4	0.00
25	54013.061576594146(272)	61.992869785(105)	-1.994516(208)	4.5(157)	2.2(101)	10	2.13
26	54129.540333159754(513)	61.990885506(113)	-1.994577(122)	12.6(55)	8.1(35)	17	0.81
27	54280.918705402011(642)	61.988307647(101)	-1.994958(89)	12.0(31)	7.7(20)	17	2.77
28	54458.695736100944(19)	61.985259013(11)	-1.995077(20)	15.0[b]	9.6[b]	11	0.54
29	54544.428887975666(21)	61.983788545(34)	-1.995050(140)	15.0[b]	9.6[b]	6	0.87
30	54582.450780475769(21)	61.983142306(16)	-1.995085(33)	15.0[b]	9.6[b]	11	0.46
31	54640.295382639395(24)	61.982153306(14)	-1.994995(24)	15.0[b]	9.6[b]	17	4.30
32	54714.291472619117(36)	61.980884633(21)	-1.995088(46)	15.0[b]	9.6[b]	10	0.84
33	54770.728789107690(24)	61.979934322(8)	-1.995453(10)	15.0[b]	9.6[b]	13	0.27
34	54914.190833277103(21)	61.977482641(5)	-1.995260(5)	15.0[b]	9.6[b]	19	0.57
35	55055.538296709147(22)	61.975059925(12)	-1.995252(26)	15.0[b]	9.6[b]	9	2.83
36	55185.431329794244(25)	61.972834648(11)	-1.995462(16)	15.0[b]	9.6[b]	14	1.22
37	55300.093397237558(200)	61.970892143(47)	-1.995418(47)	10.6(19)	6.8(12)	17	3.51
38	55457.846387537586(21)	61.968183463(14)	-1.995497(33)	15.0[b]	9.6[b]	7	1.67
39	55540.643131231653(21)	61.966763735(20)	-1.995239(146)	15.0[b]	9.6[b]	8	2.91
40	55576.371279706297(18)	61.966148592(18)	-1.994397(211)	15.0[b]	9.6[b]	7	0.42

Table 3—Continued

#	Epoch[a] (MJD)	ν (Hz)	$\dot{\nu}$ ($10^{-10} Hz\ s^{-1}$)	n	$\ddot{\nu}$ ($10^{-21} Hz\ s^{-2}$)	# fit	Reduced χ^2
41	55599.923669087368(17)	61.965747997(12)	-1.996036(187)	15.0[b]	9.6[b]	6	2.75
42	55631.577546334686(484)	61.965230243(100)	-1.995799(92)	13.2(35)	8.5(22)	14	2.09

[a]Arrival time of pulse peak in TDB.

[b]Assumed value.

Table 4. Log of PSR J0537−6910 Glitches

#	Time (MJD)	$\Delta\nu$ (μHz)	$\Delta\nu/\nu$ (ppm)	$\delta(\Delta\nu/\nu)$[a] (ppm)	ΔT_{after} (days)	Corr.[b] (days)	$\Delta T_{scatter}$ (days)	$\Delta\dot{\nu}$ (10^{-14}Hz s^{-1})	$\Delta\dot{\nu}/\dot{\nu}$ (ppm)	$\delta(\Delta\dot{\nu})/\dot{\nu}$[a] (ppm)
1	51,285.7(8.6)	42.2	0.681	0.065	283.3	-14.5	268.8	-8.4	422	622
2	51,569.0(6.8)	27.8	0.449	0.008	142.1	0.0	142.1	-14.9	746	49
3	51,711.1(6.7)	19.5	0.315	0.009	115.2	0.0	115.2	-12.1	606	74
4	51,826.3(7.1)	8.7	0.140	0.007	55.0	-11.3	43.7	-7.9	397	67
5	51,881.3(5.5)	8.7	0.141	0.020	78.8	-12.0	66.8	-3.8	188	326
6	51,960.1(4.9)	28.3	0.456	0.046	210.6	-14.0	196.6	-10.6	532	653
7	52,170.6(8.3)	11.5	0.185	0.006	71.0	0.0	71.0	-12.8	642	25
8	52,241.6(7.8)	26.5	0.427	0.006	144.4	0.0	144.4	-3.4	170	44
9	52,386.0(5.7)	10.4	0.168	0.020	67.3	0.0	67.3	-12.1	607	242
10	52,453.3(6.9)	13.5	0.217	0.030	92.5	0.0	92.5	-6.8	342	355
11	52,545.3(6.2)	26.1	0.421	0.018	194.0	-22.6	171.4	-7.1	357	175
12	52,739.8(5.3)	9.0	0.144	0.006	79.2	-20.5	58.7	-11.2	564	29
13	52,819.0(3.6)	15.9	0.256	0.016	67.9	0.0	67.9	-8.0	401	212
14	52,886.9(4.5)	14.5	0.234	0.023	127.1	0.0	127.1	-11.2	562	263
15	53,014.0(9.5)	21.0	0.338	0.010	111.4	0.0	111.4	-14.1	708	78
16	53,125.4(2.8)	1.1	0.018	0.014	19.8	0.0	19.8	-12.4	620	243
17	53,145.2(2.7)	24.3	0.392	0.008	143.1	0.0	143.1	2.05	-102	230
18	53,288.3(2.4)	24.5	0.395	0.010	157.3	-3.2	154.1	-13.5	677	58
19	53,445.6(1.7)	16.1	0.259	0.016	105.2	-10.4	94.8	-14.1	705	125
20	53,550.8(4.4)	19.9	0.322	0.026	156.4	-22.8	133.6	-11.8	590	205

Table 4—Continued

#	Time (MJD)	$\Delta\nu$ (μHz)	$\Delta\nu/\nu$ (ppm)	$\delta(\Delta\nu/\nu)$[a] (ppm)	ΔT_{after} (days)	Corr.[b] (days)	$\Delta T_{scatter}$ (days)	$\Delta\dot{\nu}$ (10^{-14}Hz s^{-1})	$\Delta\dot{\nu}/\dot{\nu}$ (ppm)	$\delta(\Delta\dot{\nu})/\dot{\nu}$[a] (ppm)
21	53,699.2(3.9)	24.9	0.402	0.008	161.4	-17.9	143.5	-12.8	640	173
22	53,860.1(1.5)	14.5	0.235	0.020	91.1	-14.6	76.5	-12.4	625	146
23	53,951.2(1.5)	1.1	0.018	0.020	47.9	-27.5	20.4	-13.0	651	137
24	53,999.1(3.4)	22.5	0.362	0.020	108.8	-14.0	94.8	-4.5	224	154
25	54,107.9(8.0)	23.0	0.369	0.020	167.1	-21.5	145.6	—	—	—
26	54,275.0(2.0)	30.3	0.489	0.020	169.8	0.0	169.8	—	—	—
27	54,445.0(3.6)	14.8	0.239	0.020	91.3	-5.6	85.7	-13.2	662	73
28	54,539.9(1.9)	7.2	0.145	0.020	33.4	0.0	33.4	-7.4	370	256
29	54,576.2(2.9)	9.1	0.160	0.020	62.4	0.0	62.4	—	—	—
30	54,638.7(1.6)	8.0	0.129	0.020	73.6	0.0	73.6	—	—	—
31	54,712.3(2.0)	6.6	0.106	0.020	56.5	0.0	56.5	—	—	—
32	54,768.8(1.9)	22.4	0.361	0.020	122.2	0.0	122.2	—	—	—
33	54,891.0(5.7)	21.3	0.344	0.060	146.1	0.0	146.1	—	—	—
34	55,046.8(2.0)	13.4	0.197	0.020	134.9	-54.2	80.7	—	—	—
35	55,183.5(2.0)	13.0	0.210	0.020	85.7	0.0	85.7	—	—	—
36	55,269.2(6.0)	34.2	0.552	0.020	182.1	0.0	182.1	—	—	—
37	55,451.3(6.0)	10.5	0.169	0.020	67.1	0.0	67.1	—	—	—
38	55,518.7(6.0)	7.6	0.123	0.020	37.2	0.0	37.2	—	—	—
39	55,555.9(6.0)	0.63	0.010	0.020	30.9	0.0	30.9	—	—	—
40	55,589.3(2.5)	5.5	0.139	0.020	28.5	0.0	28.5	—	—	—

Table 4—Continued

#	Time (MJD)	$\Delta\nu$ (μHz)	$\Delta\nu/\nu$ (ppm)	$\delta(\Delta\nu/\nu)$[a] (ppm)	ΔT_{after} (days)	Corr.[b] (days)	$\Delta T_{scatter}$ (days)	$\Delta\dot{\nu}$ (10^{-14}Hz s^{-1})	$\Delta\dot{\nu}/\dot{\nu}$ (ppm)	$\delta(\Delta\dot{\nu})/\dot{\nu}$[a] (ppm)
41	55,614.7(4.0)	28.2	0.454	0.020	>164.3	0.0	>164.3	—	—	—
Average		16.8	0.272		108.0	-7.2	100.8	-9.9	498	

[a]These errors come from the formal errors on ν and $\dot{\nu}$ of the polynomial fits.

[b]Days needed to convert the time to the next glitch into the time to the beginning of quasi-stable behavior.

Table 5. Log of Large Glitches from other Pulsars

PSR J	Time (MJD)	ν (Hz)	$\Delta\nu$ (μHz)	$\Delta\nu/\nu$ (ppm)	$\dot{\nu}$ (fHz/s)	-$\Delta\dot{\nu}$ (fHz/s)	$\Delta\dot{\nu}/\dot{\nu}$ (10^{-3})	Q (10^{-3})	Ref.[a]
0205+6449	52,555(13)	15.22230	5.18(167)	1.0 (1)	-44956.	224.8(45.0)	– – – –	– – – –	1
	52,920(72)	15.22230	54.79(610)	1.0 (1)	-44956.	539.5(45.0)	– – – –	– – – –	2,3
0358+5413	46,497(4)	6.39463	27.93(1)	4.638(1)	-179.8	12.6(1.8)	70(10)	1.12(7)	3,4
0534+2200	53,067(0)	29.79695	6.38(3)	0.214(1)	-3753.4	2327.1(751)	6.2(2)	– – – –	3
0631+1036	50,729(1)	3.47463	5.78(3)	1.6627(1)	-1263.74	4.4(3)	3.5(2)	– – – –	3
0729-1448	54,687(3)	3.47463	26.53(4)	6.6767(9)	-1788.79	96.6(89)	5.4(5)	– – – –	3
0835-4510	40,280(4)	11.20978	26.23(11)	2.340(10)	-16326.	115.1	7.08[b]	30(10)	5,6
	41,192(8)	11.20855	22.98(34)	2.050(30)	-16257.	117.9	7.25[b]	35.(1)	5,6
	42,683(3)	11.20654	22.30(11)	1.990(10)	-16145.	114.	7.1[b]	88.(8)	5,6,7
	43,693(12)	11.20518	34.29(67)	3.060(60)	-16069.	104.1	6.48[b]	24.(5)	5,6,7
	44,888(0)	11.20357	12.83(3)	1.145(3)	-15980.	102.	6.39[b]	183.(1)	5,8
	45,192(1)	11.20316	22.97(11)	2.050(10)	-15956.	97.	6.1[b]	44.(3)	5,9
	46,257(0)	11.20173	17.93(11)	1.601(1)	-15875.	103.	6.5[b]	158.(1)	9
	47,520(0)	11.20000	20.24(1)	1.807 (1)	-15780.	68.2	4.32[b]	– – – –	10,11
	48,457(0)	11.19877	30.40(2)	2.715 (2)	-15709.	– – – –	– – – –	– – – –	12
	49,559(0)	11.19729	9.35(2)	0.835 (2)	-15626.	– – – –	– – – –	– – – –	13
	50,369(0)	11.19620	23.62(13)	2.110(12)	-1556.5	92.6(5)	5.95(3)	380(2)	14
	51,559(0)	11.19242	34.54(0)	3.086(0)	-1556.1	104.8(0)	– – – –	– – – –	15
	53,193(0)	11.19465	23.51	2.100	-1556.1	– – – –	– – – –	– – – –	16
	53,960(0)	11.19142	29.32(0)	2.620(0)	-1555.0	3577.(622)	230(40)	– – – –	17

Table 5—Continued

PSR J	Time (MJD)	ν (Hz)	$\Delta\nu$ (μHz)	$\Delta\nu/\nu$ (ppm)	$\dot{\nu}$ (fHz/s)	-$\Delta\dot{\nu}$ (fHz/s)	$\Delta\dot{\nu}/\dot{\nu}$ (10^{-3})	Q (10^{-3})	Ref.[a]
1048-5832	49,034(9)	8.08700	24.22(4)	2.995(7)	-6235.1	23.1(6)	3.7(1)	2.5(3)	18
	50,791(5)	8.08604	6.22(6)	0.771(7)	-6236.0	28.8(4)	4.62(6)	– – – –	19
1341-6220	47,989(10)	5.17376	7.78(4)	1.505(8)	-6774.3	1.0(4)	0.15(6)	≤1	20
	48,645(5)	5.17352	5.12(4)	0.990(3)	-6775.9	4.7(7)	0.7(1)	2.0(3)	20
	50,008(16)	5.17274	8.46(7)	1.636(13)	-6771.5	2.2(3)	3.3(4)	4	20
1357-6429	52,012(16)	6.02118	14.60(10)	2.420(20)	-1307.4	70.2(3)	5.37(2)	– – – –	21
1539-5626	48,465(10)	4.1086	11.47(8)	2.791(2)	-81.9	4. (1.)	0.4(1)	≤1	22
1614-5048	49,803(16)	4.31688	27.87(28)	6.456(65)	-9241.8	89.6(1.8)	9.7(2)	538(11)	18
1617-5055	46,960(760)	14.41819	8.65(7)	600(5)	2809.	– – – –	– – – –	– – – –	23
1709-4429	48,780(15)	9.76095	19.64(8)	2.0123(2)	-8891.7	1.8(5)	0.20(6)	133(7)	22
1730-3350	47,990(10)	7.1714	22.10(7)	3.080(10)	-4643.4	56. (14)	12.(3)	8(1)	22
	52,107(9)	7.1714	22.96(1)	3.202(1)	-4361.6	257. (4)	5.9(1)	8(1)	3
1801-2451	49,476(6)	8.00694	16.00(6)	1.998(7)	-8172.6	39.2(3)	4.8(3)	188(12)	18,24
	50,651(5)	8.00612	9.90(3)	1.237(4)	-8206.9	31.7(7)	3.87(9)	202(6)	18
	52,055(0)	8.00612	30.06(0)	3.756(0)	-8195.9	55.7(6)	6.8 (1)	202(6)	18,3
	54,661(2)	8.00612	24.82(0)	3.101(0)	-8195.9	76.2(7)	9.3 (1)	202(6)	18,3

Table 5—Continued

PSR J	Time (MJD)	ν (Hz)	$\Delta\nu$ (μHz)	$\Delta\nu/\nu$ (ppm)	$\dot{\nu}$ (fHz/s)	-$\Delta\dot{\nu}$ (fHz/s)	$\Delta\dot{\nu}/\dot{\nu}$ (10^{-3})	Q (10^{-3})	Ref.[a]
1803-2137	48,245(10)	7.4849	30.50(11)	4.075(15)	-7536.2	69.3(3)	9.2(4)	15(2)	5
	50,765(15)	7.48326	23.95(20)	3.200(27)	-7488.9	79.7(11)	10.7(15)	161(6)	14,3
	53,429(1)	7.48128	29.40(0)	3.929(7)	-7520.0	79.7(11)	10.6(1)	– – ––	18,3
1806-2125	51,062(242)	2.0756	32.41(02)	15.615(15)	-505.9	17.(2)	33.6(40)	– – ––	25
1809-1917	53,251(2)	12.0850	19.64(0)	1.625(0)	3729.4	290.9 (120)	7.8(3)	– – ––	3
1824-1118	54,306(3)	2.2948	6.602(2)	2.877(0)	-18.7	1.9 (4)	10(2)	– – ––	3
1826-1334	46,507(40)	9.85827	26.79(49)	2.718(26)	-7275.6	72. (7)	6.8(1)	– – ––	5,3
	49,014(40)	9.8567	30.16(49)	3.060(50)	-7235.4	72. (7)	10(1)	18(1)	5,3
	53,737(1)	9.8535	35.28(1)	3.581(1)	-7235.4	69.5(28)	9.6(4)	– – ––	5,3
1833-0827	48,041(10)	11.7258	21.87(2)	1.8648(3)	-1260.6	1.93(6)	1.53(4)	0.8(2)	5,3
1838-0453	53,388(10)	2.6258	26.00(100)	9.902(381)	-797.5	5.58(80)	7(1)	– – ––	3
1846-0258	53,883(2)	3.70458	22.97(111)	6.200(300)	-66799.3	297.9(1.3)	4.46(2)	– – ––	2,26
1856+0113	54,123(10)	3.7392	43.17(0)	11.569(1)	-2913.1	64.08(64)	22(2)	– – ––	3
1932+2220	46.906(85)	6.92221	30.64(5)	4.427 (7)	-2758.4	– – ––	– – ––	– – ––	3
	50,253(4)	6.92221	30.85(5)	4.457 (6)	-2756.4	4.7 (5)	1.7 (2)	– – ––	27,3
2021+3651	52,630(0)	9.64114	24.94(2)	2.587 (2)	-8886.5	55. (3)	6.2 (5)	– – ––	28
	54,177(25)	9.63939	7.181(2)	0.745 (6)	-8886.5	48.9 (9)	5.5 (1)	– – ––	3

Table 5—Continued

PSR J	Time (MJD)	ν (Hz)	$\Delta\nu$ (μHz)	$\Delta\nu/\nu$ (ppm)	$\dot{\nu}$ (fHz/s)	-$\Delta\dot{\nu}$ (fHz/s)	$\Delta\dot{\nu}/\dot{\nu}$ (10^{-3})	Q (10^{-3})	Ref.[a]
2229+6114	55,064(3)	19.37104	22.07(1)	1.1393(3)	-2937.	3.67 (3)	12.5 (1)	– – ––	3
	54,110(1)	19.37104	6.33(1)	0.327 (4)	-2937.	3.67 (3)	-3 (6)	– – ––	3
2337+6151	53,642(3)	2.01898	41.33(1)	20.470(3)	-782.	18.6 (4)	23.8 (4)	– – ––	29,3

[a]Refs: 1. Ransom et al. (2004); 2. Livingstone et al. (2009); 3. Espinoza et al. (2011); 4. Lyne (1987); 5. Shemar & Lyne (1996); 6. Cordes, Downs, & Krause-Polstorff (1988); 7. Downs (1981); 8 Manchester et al. (1983); 8. McCulloch et al. (1983); 9. McCulloch et al. (1987); 10. Flanagan (1990); 11. McCulloch et al. (1990); 12. Flanagan (1991); 13. Flanagan (1994a); 14. Flanagan (1994b); 15. Dodson, McCulloch, & Lewis (2002); 16. Dodson et al. (2004); 17. Flanagan & Buchner (2006); 18. Wang et al. (2000); 19. Urama (2002) 20. Kaspi et al. (1992) 21. Camilo et al. (2004); 22. Johnston et al. (1995); 23. Torii et al. (2000) 24. Arzoumanian et al. (1994); 25. Hobbs et al. (2002); 26. Kuiper & Hermsen (2009) 27. Krawczyk, et al. (2003); 28. Hessels et al. (2004); 29. Yuan et al. (2010).

[b]These values are the part of the spindown jump associated with the long term recovery and are taken from Alpar et al. (1993).

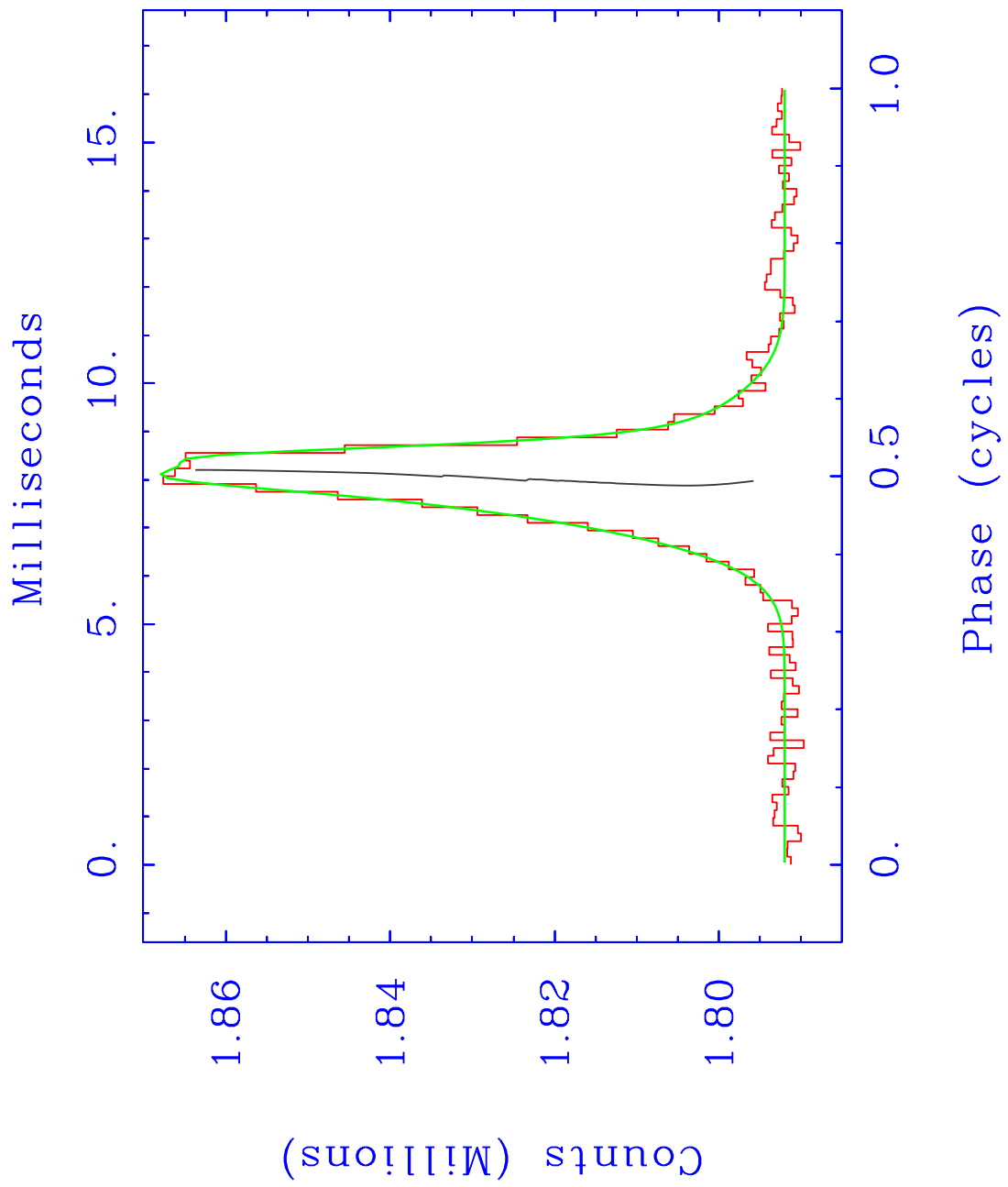

Fig. 1.— The pulse profile for PSR J0537−6910 from 311 observations taken during the RXTE campaign from Jan. 19, 1999, to Oct. 6, 2004. The parameters of the MPP curve drawn over the summed data are listed in Table 2. The vertical curve marks the midpoint of the pulse profile vs. height.

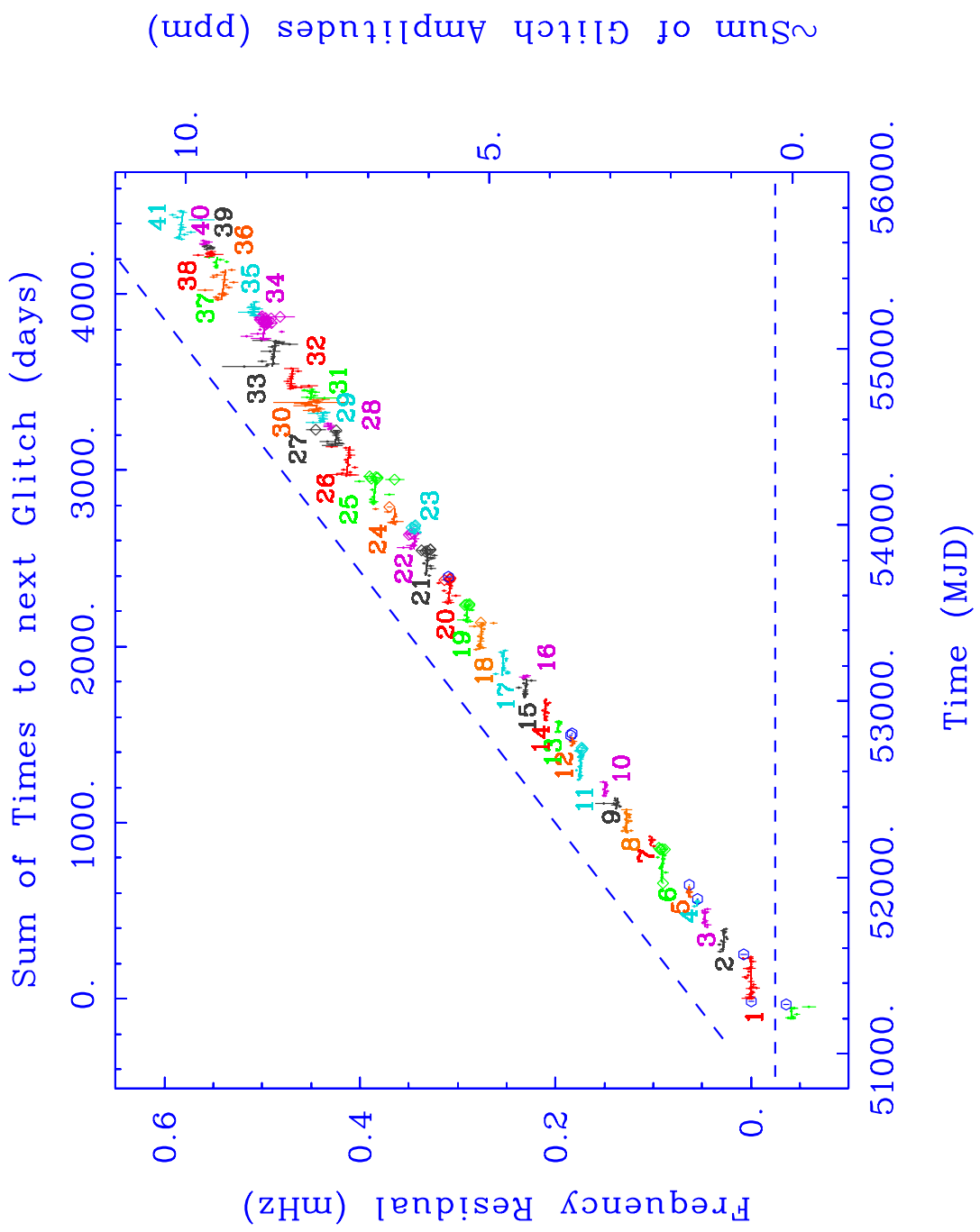

Fig. 2.— The frequency history for PSR J0537−6910. The frequency measurements of the individual observations are shown with error bars. The (mostly horizontal) curves are the frequency histories derived from the much more accurate timing solutions. The right frame boundary labels the *approximate* cumulative gain of frequency across the glitches (see Fig. 8). Diamonds mark points with known phases from the timing solutions, but which were not included in them. Hexagons mark observations for which no timing solution exists. The horizontal dashed line is the baseline for the frequency residuals, and corresponds to $62.037465 - 1.9922\times10^{-10}\times(\mathrm{MJD} - 51{,}400)\times86400$ Hz. The oblique dashed line is an approximation to the mean trend for the frequency residuals, and corresponds to $62.037545987 - 1.9760\times10^{-10}\times(\mathrm{MJD} - 51{,}400)\times86400$ Hz.

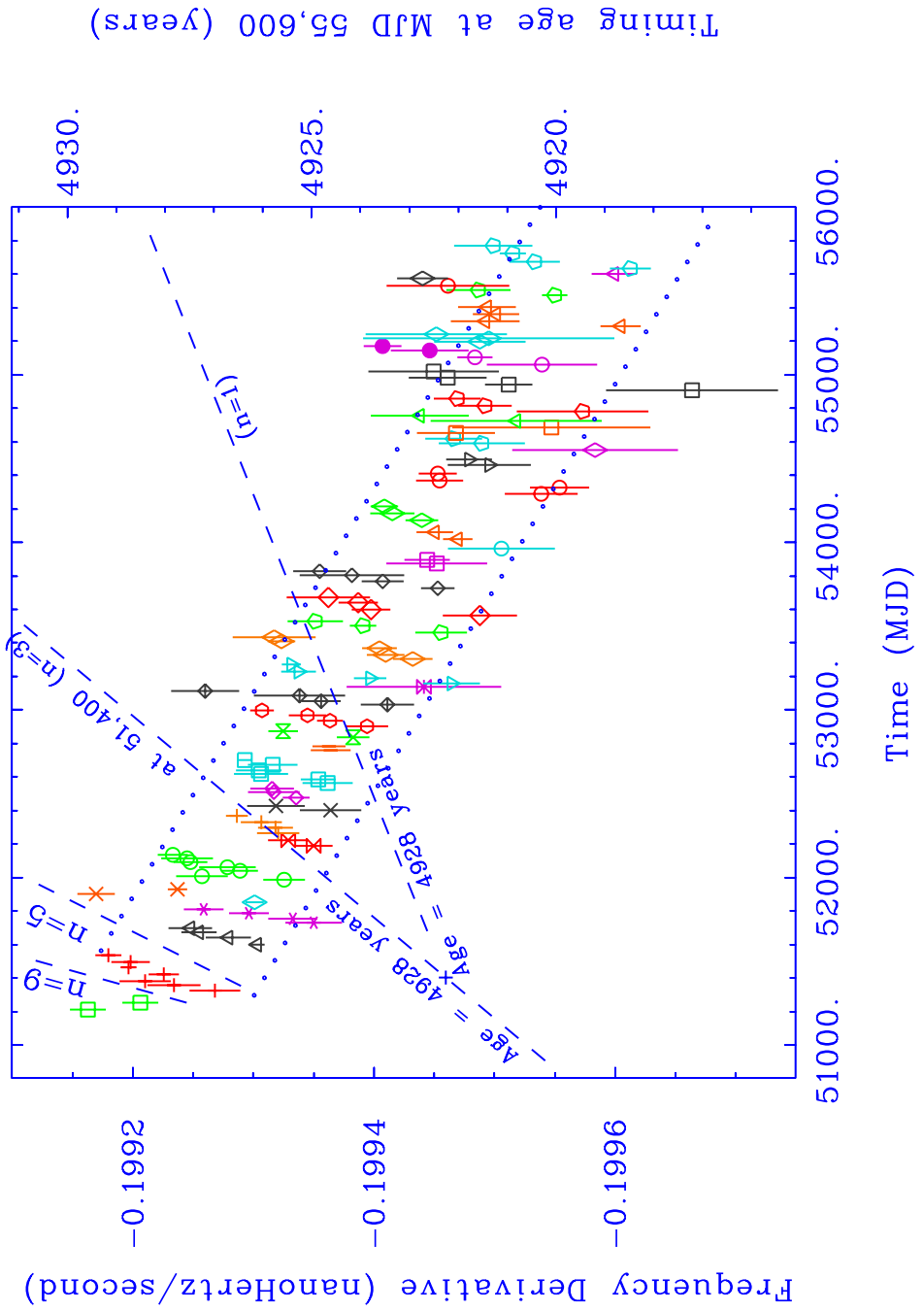

Fig. 3.— The $\dot{\nu}$ or spindown history for PSR J0537−6910, derived from subsegments of at least three consecutive observations with a time span of at least 1,400,000 s (with the exception of the 17th data segment, which only spanned 14 days), and at least one observation within 0.35 of the full time span of its center. The two dotted lines are spaced at 0.15 pHz s^{-1} and slope downward at 0.95×10^{-21} Hz s^{-2}, or 0.15 pHz s^{-1} (five years)$^{-1}$, or a braking index, n, of -1.5.

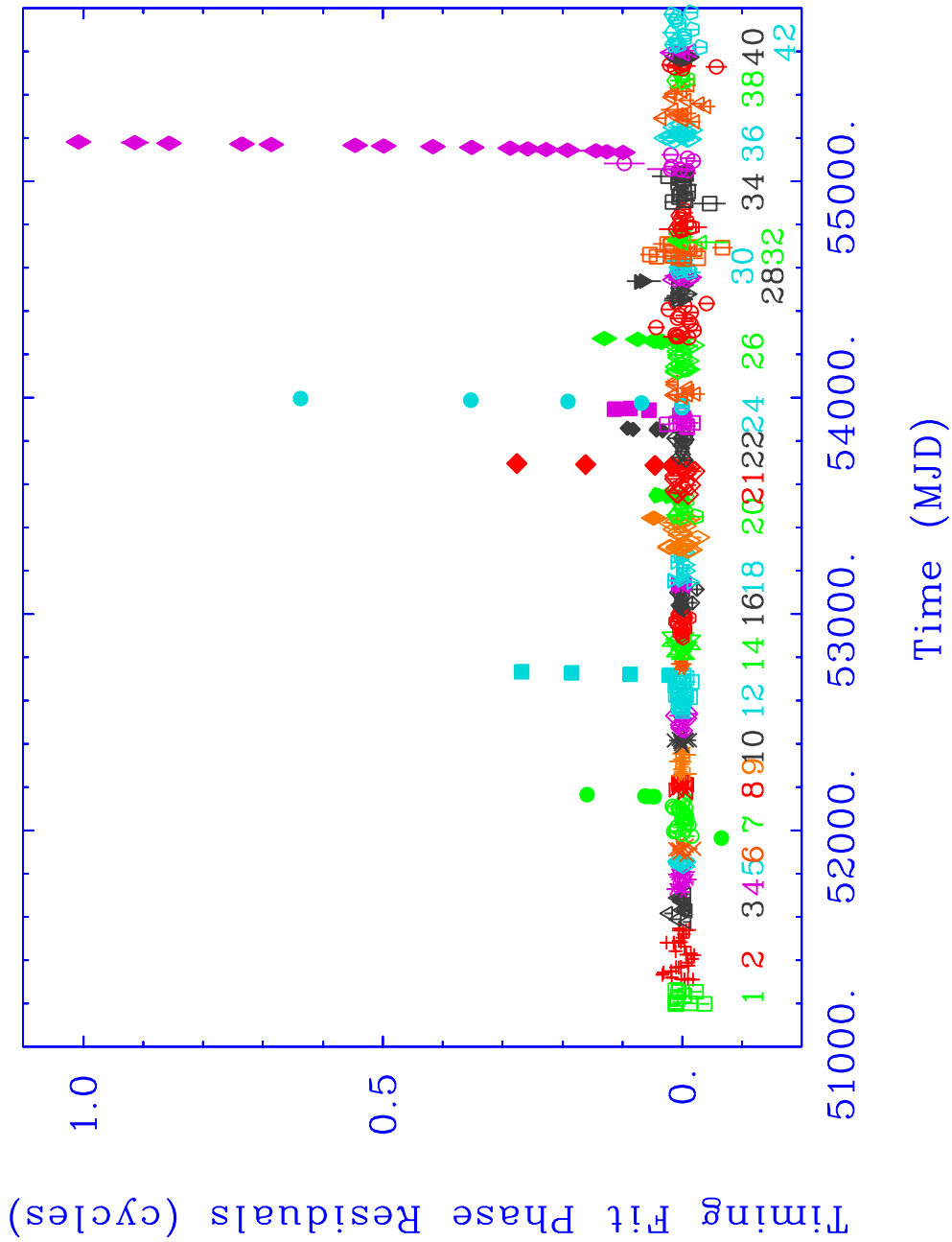

Fig. 4.— The phase residuals to the timing solution fits for all 24 data segments, with the segment numbers listed just below the corresponding residuals. The solid points have not been included in the fits. The residuals for observations with no timing solutions have not been plotted.

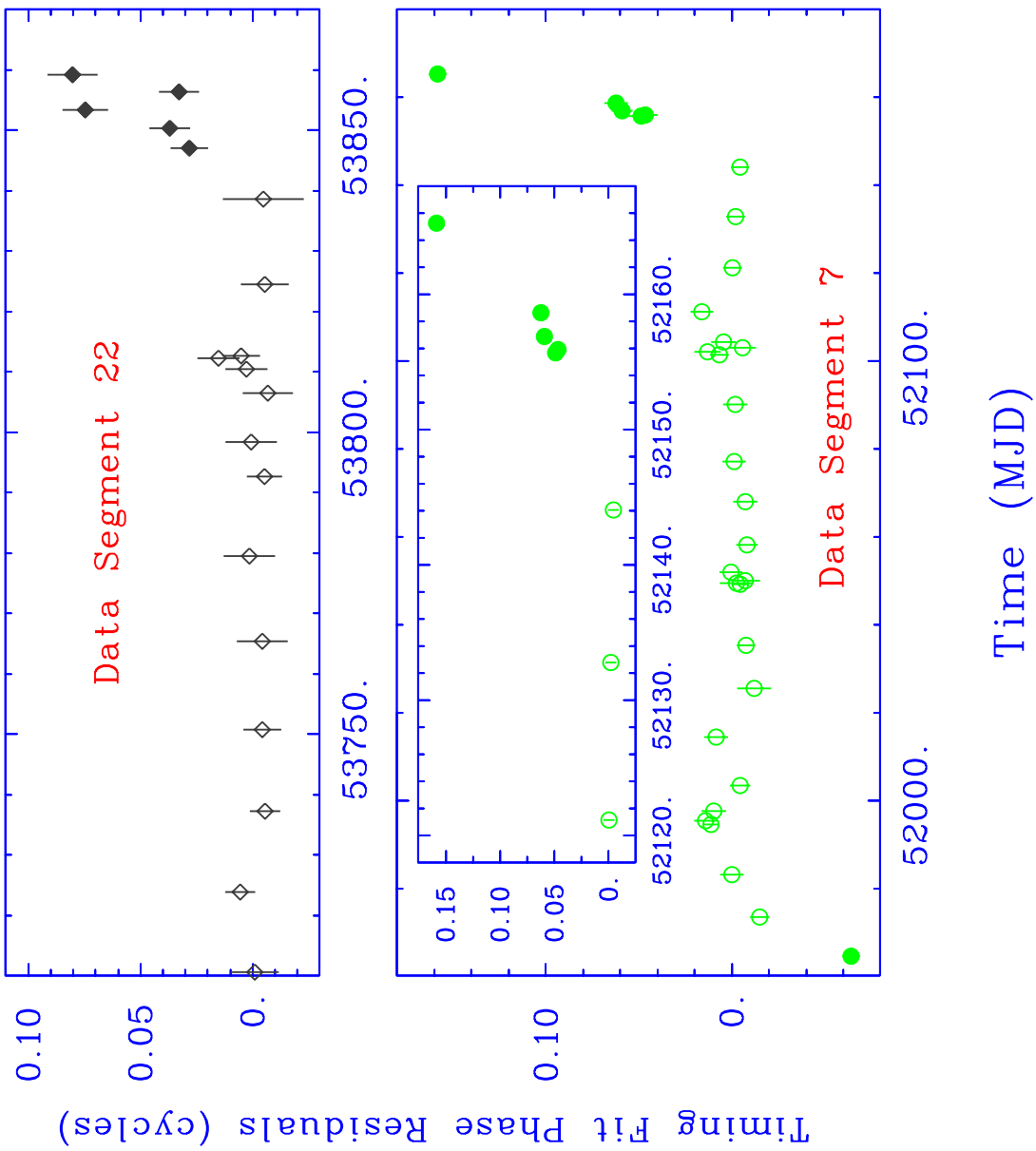

Fig. 5.— (Lower) The timing residuals for data segment 7. The solid points have not been included in the fit. (Upper) The timing residuals for data segment 22.

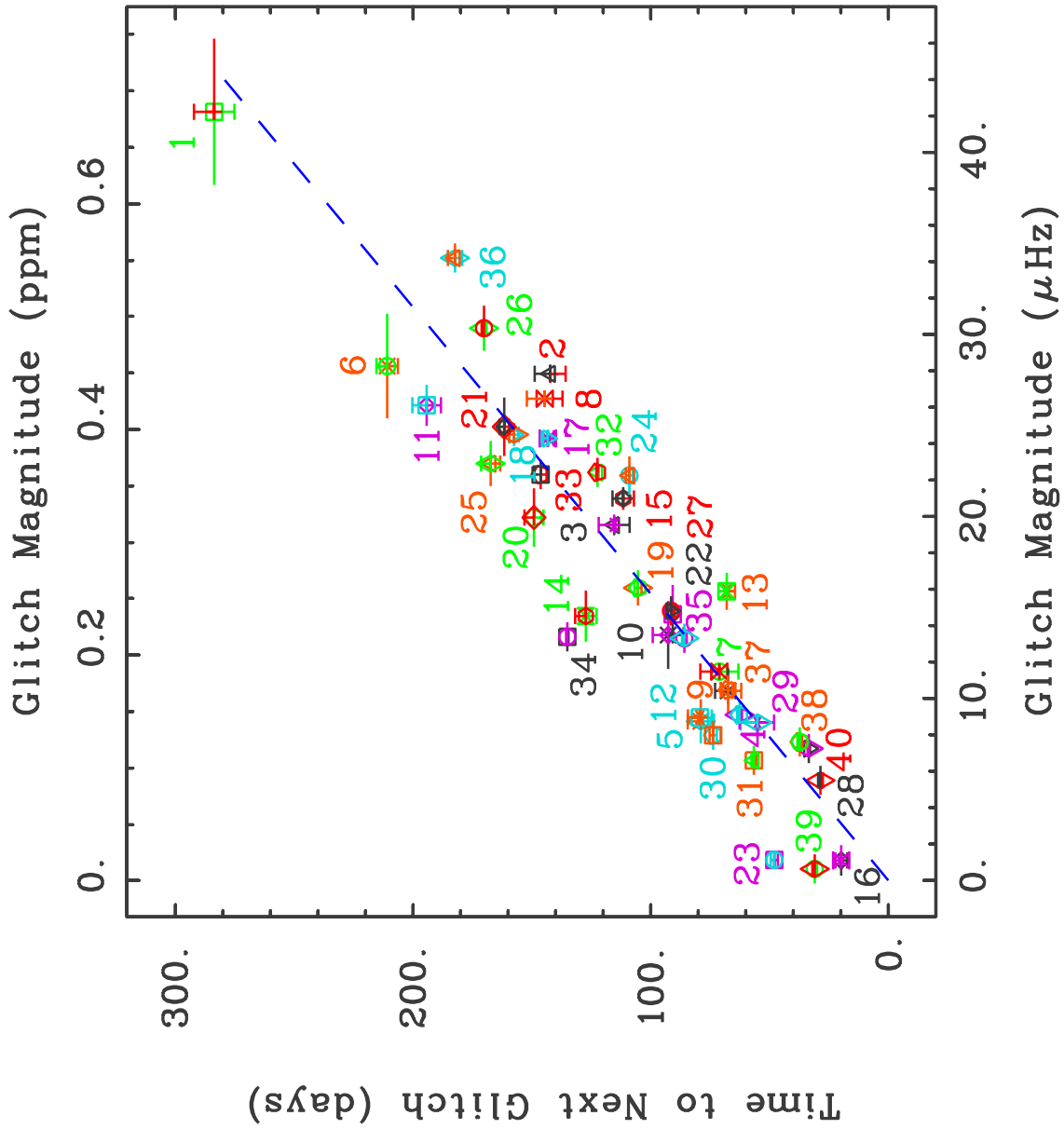

Fig. 6.— The glitch amplitude vs. the time to the next glitch (see Table 4). The time bounds drawn for the points are equal (up and down) and each is a quarter of the sum of two time intervals bounding the data segment. The slope of the dashed line fitted to the points and through the origin is 6.3411 days μHz^{-1}, or 393.22 days ppm^{-1} assuming a mean frequency of 62.00 Hz.

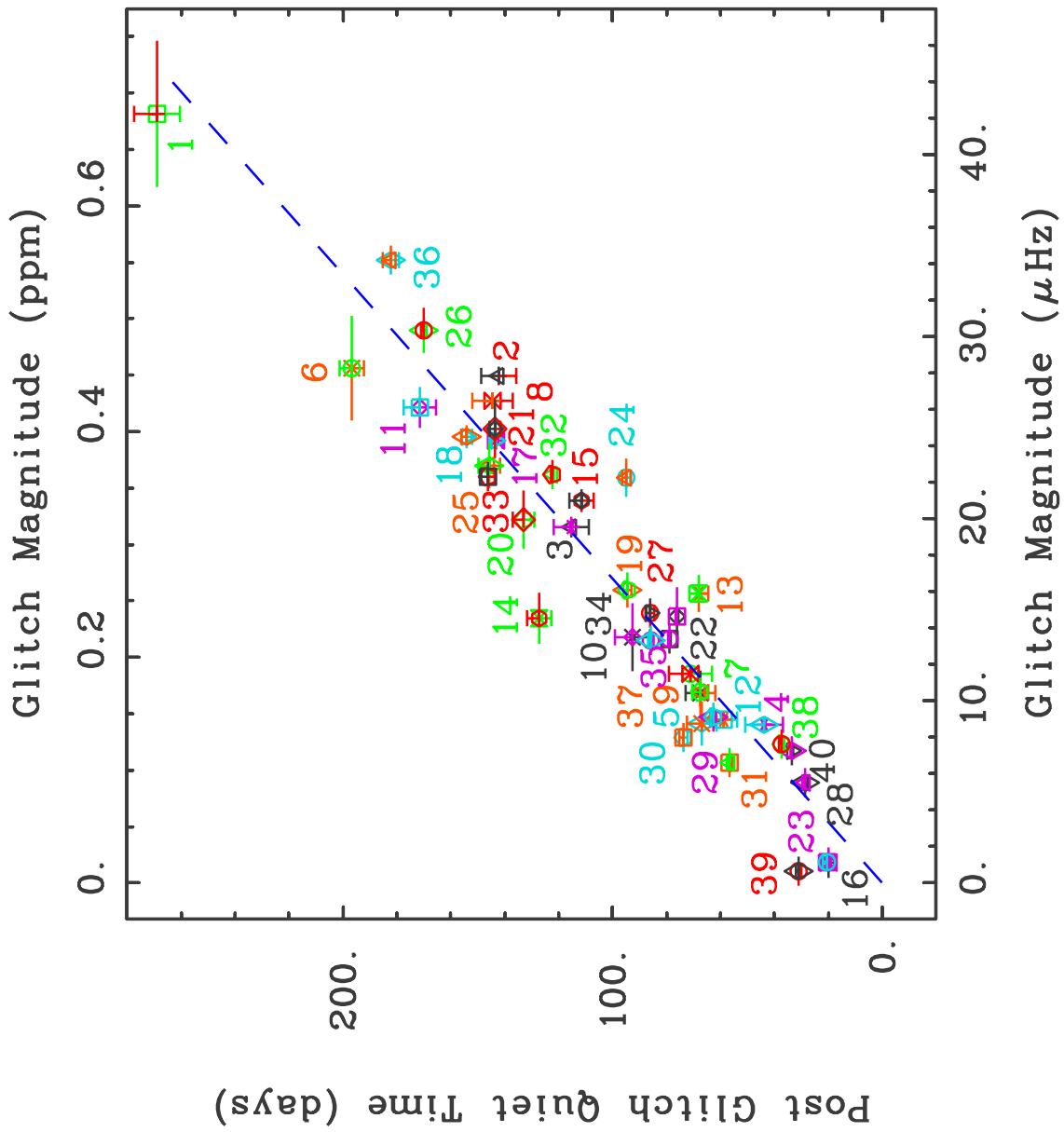

Fig. 7.— The glitch amplitude vs. the following interval of stable timing behavior (see Table 4). The slope of the dashed line fitted to the points and through the origin is 5.9811 days μHz^{-1}, or 370.83 days ppm^{-1} assuming a mean frequency of 62.00 Hz. Glitches 9 and 37 very nearly overlay.

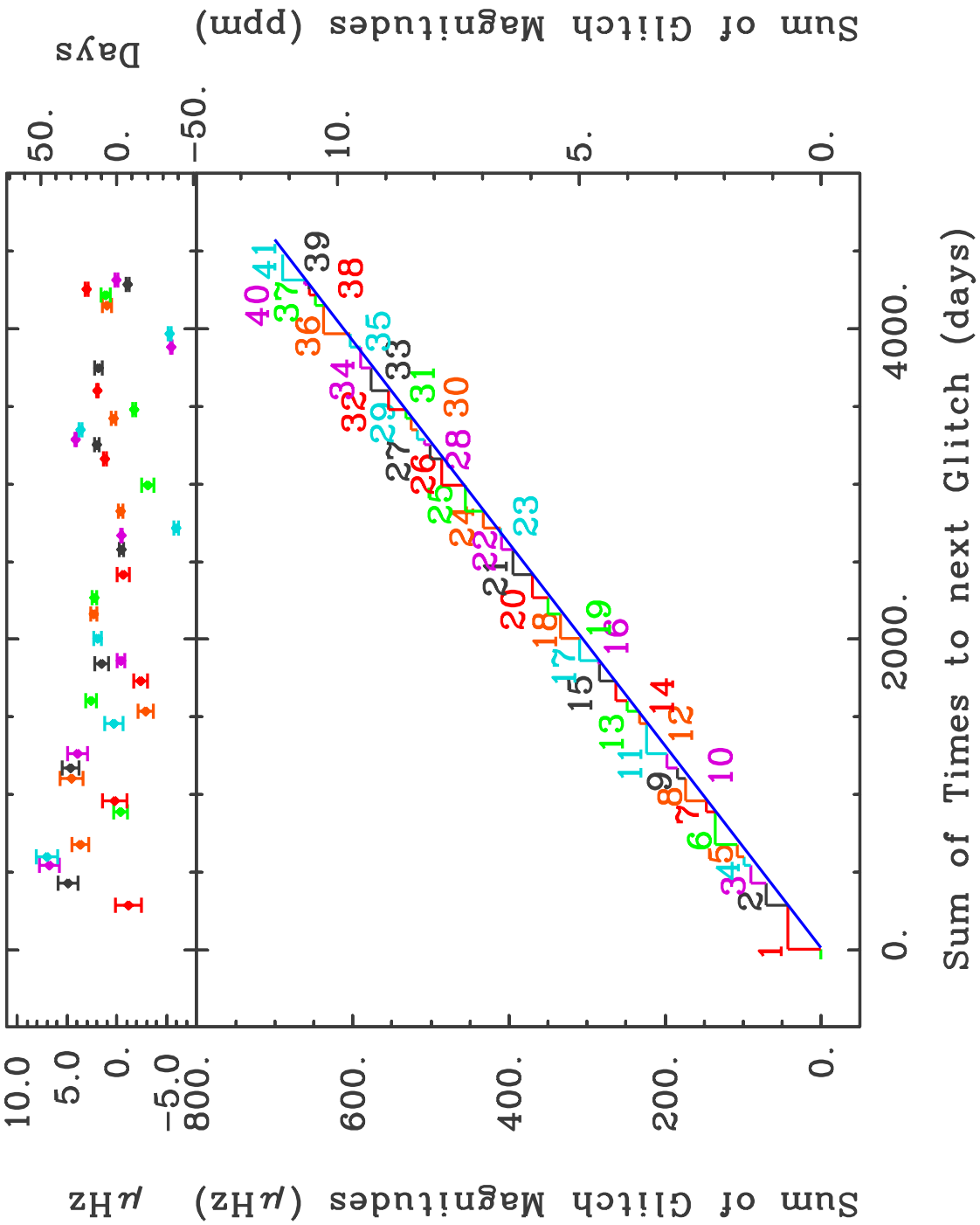

Fig. 8.— Cumulative time vs. cumulative glitch amplitude. The oblique line drawn from (0,0) to the bottom of glitch 41 has been offset from the first and last glitch times by ten days for clarity, and has a slope of 6.5229 days μHz^{-1} or 404.418 days ppm^{-1} assuming a mean frequency of 62.00 Hz. The top frame plots the predicted glitch onset time minus the actual glitch onset time (in days on the right hand scale, and converted to equivalent μHz on the left hand scale).

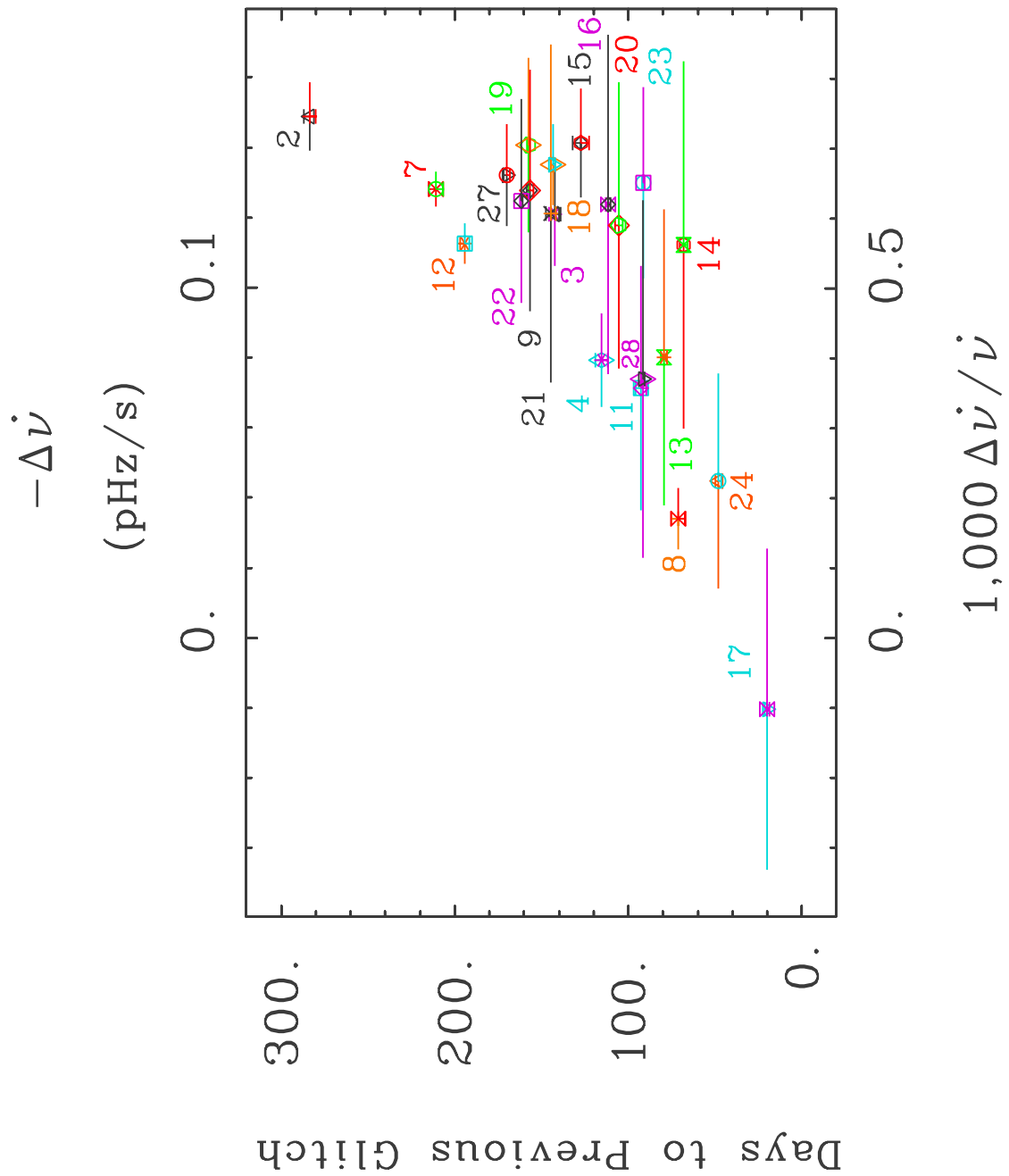

Fig. 9.— The time to the previous glitch vs. $\Delta\dot{\nu}$ across the glitch. Glitches 5, 6, 10, 25, and 26 have been omitted due to large errors in $\Delta\dot{\nu}$ (see Table 4).

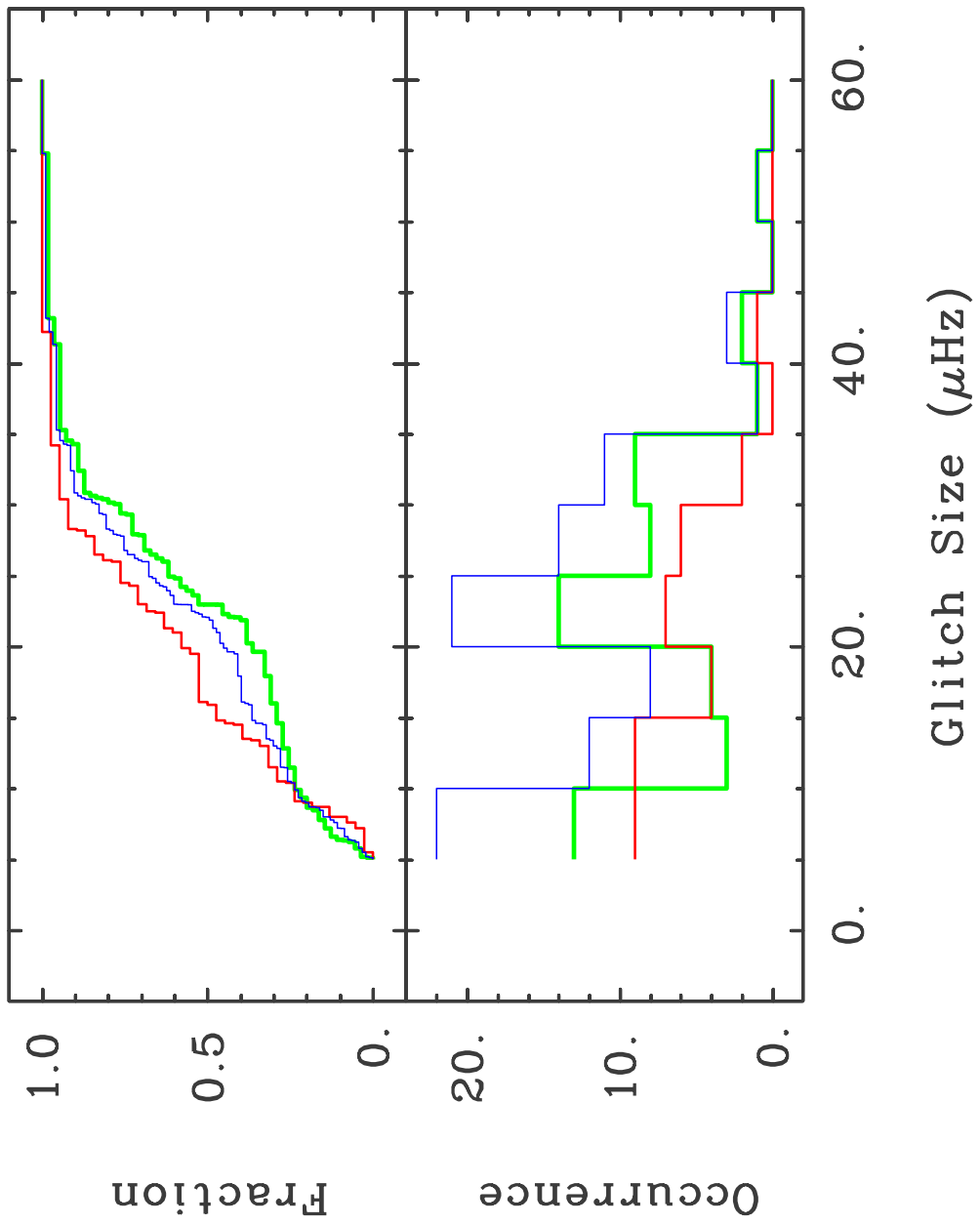

Fig. 10.— The distribution in size of 36 large glitches from PSR J0537−6910 (medium thickness line), and 34 more glitches from other pulsars (thick line), all larger than 5 μHz, in addition to the combination of both samples (thin line).

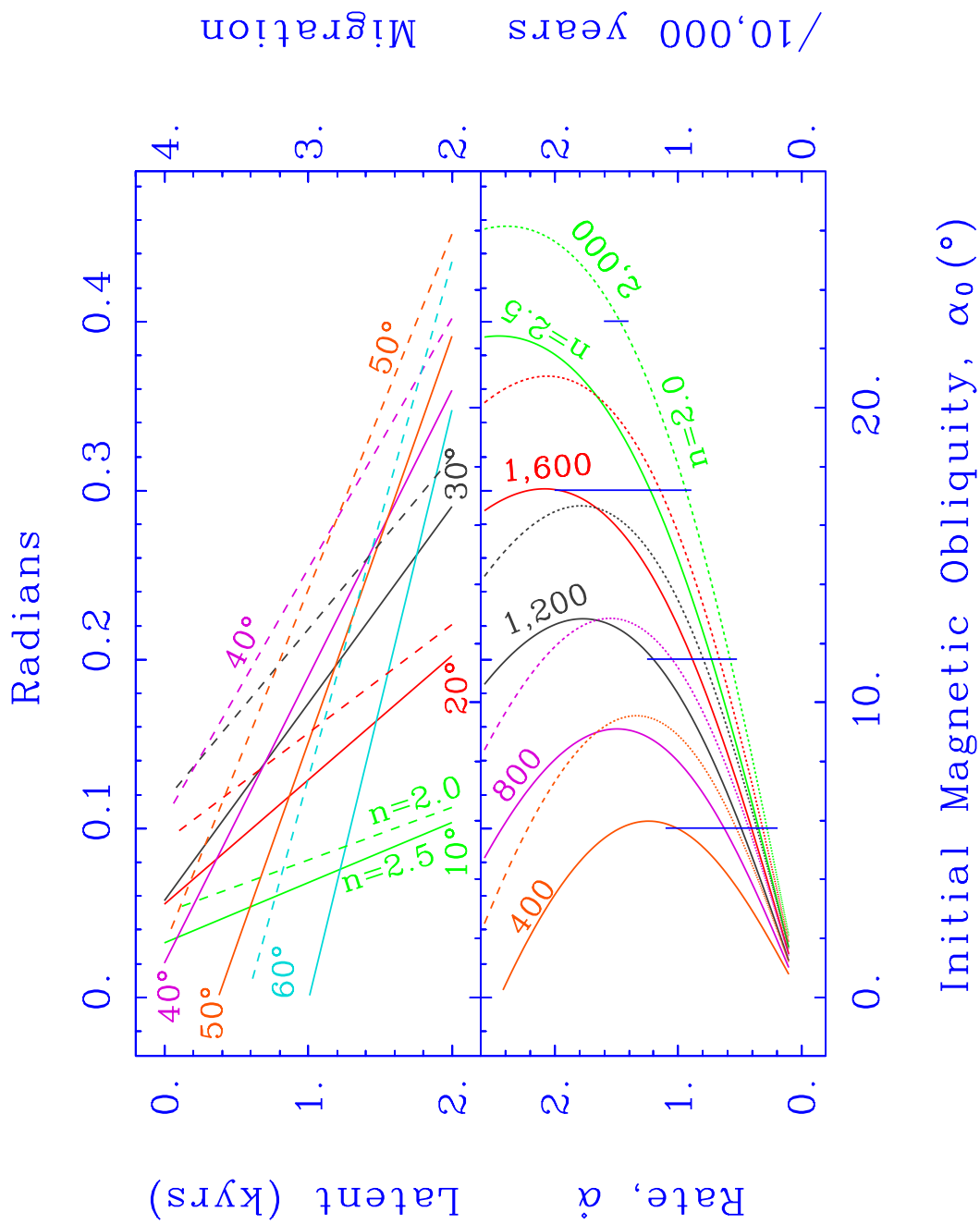

Fig. 11.— (Lower) The magnetic pole migration rate vs. initial obliquity of PSR J0537−6910 for an age of 4,000 years, latency times (with no polar migration) from 2,000 to 3,600 years in steps of 400 years, and two values of the (intrinsic) braking index, n, 2.5 (solid) and 2.0 (dotted/dashed). The four vertical lines of constant initial obliquity, or α_0, intersect the curves at 22 migration rates, or $\dot{\alpha}$'s, for which time histories of ν and $\dot{\nu}$ are plotted in Fig. 12 (see § 5.2.3). (Upper) Lines of constant present day magnetic obliquity, assuming a 4,000-year age for PSR J0537−6910, for braking indices 2.5 (solid) and 2.0 (dashed) are plotted on the initial obliquity-time plane. See Fig. 12 and § 5.2.3.

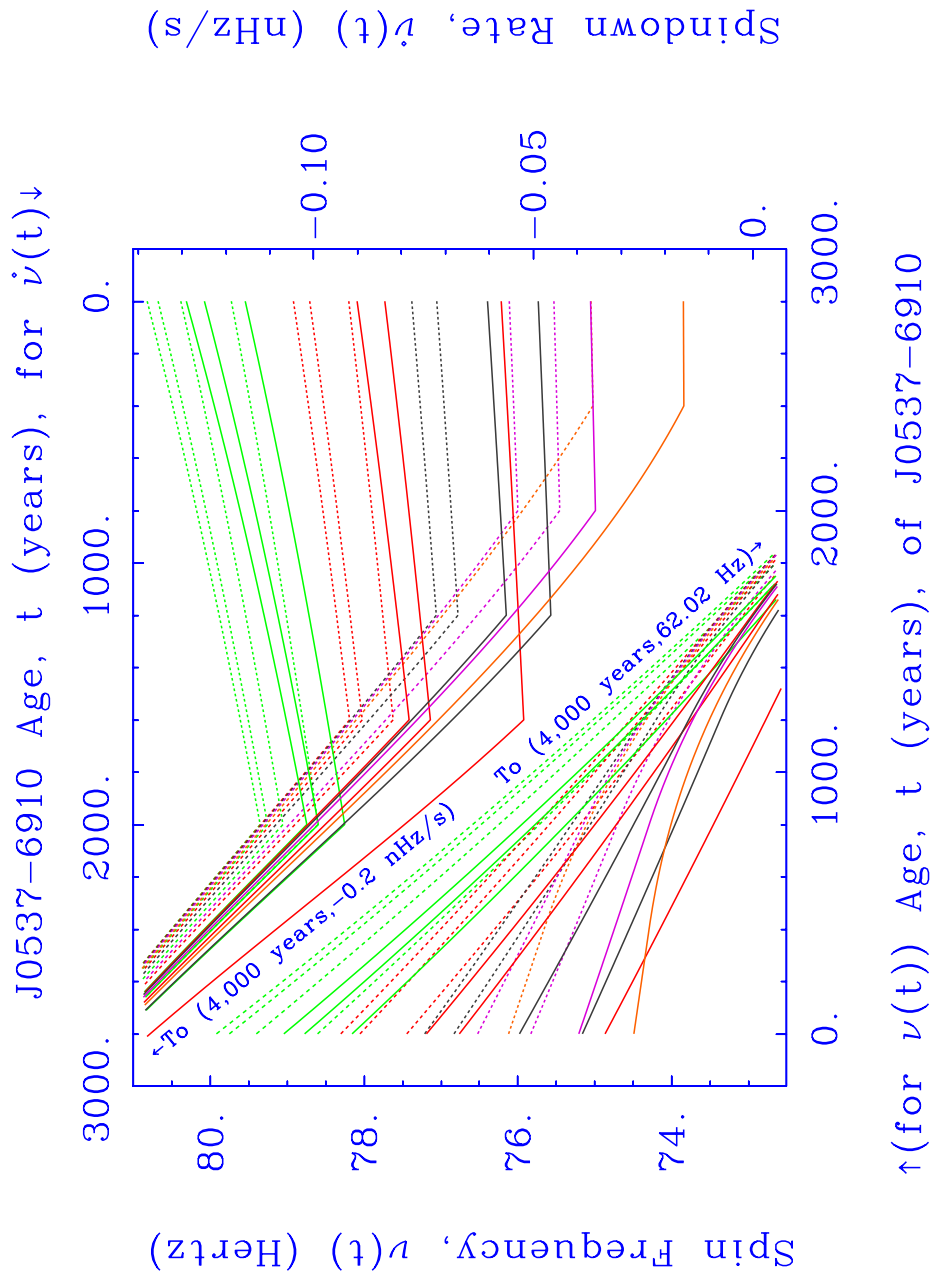

Fig. 12.— Segments of 22 possible time histories of PSR J0537−6910 for a present age of 4,000 years, and for parameters from the intersections of ordinates of Fig. 11 representing initial magnetic obliquities of 0.1 – 0.4 radians in steps of 0.1 radians, with the lower migration rate segments of curves of constant pole-migration intervals from 2000 to 3600 years in steps of 400 years, and braking indices, n, of 2.5 (solid) and 2.0 (dotted – see Fig. 11). The pulse frequency, ν, histories are curves with values labeled on the left hand and bottom frame boundaries, first visible at the bottom center and continuing left/backward in time, while rising to the left-hand frame edge. The curves with the slope breaks are spindown histories and are labeled on the top and right-hand sides.